7-20-2021

Reduced-order Modeling of Loosening in Bolted Joints and Dynamic Interactions Between Axially Aligned Threaded Joints

Sandro Aldana
University of Nebraska-Lincoln, saldana2@huskers.unl.edu

Reduced-order Modeling of Loosening in Bolted Joints and Dynamic Interactions Between Axially Aligned Threaded Joints

By

Sandro A. Aldana

A THESIS

Presented to the Faculty of

The Graduate College at the University of Nebraska

In Partial Fulfillment of Requirements

For the Degree of Master of Science

Major: Mechanical Engineering & Applied Mechanics

Under the Supervision of Professor Keegan J. Moore

Lincoln, Nebraska

August, 2021

Reduced-order Modeling of Loosening in Bolted Joints and
Dynamic Interactions Between Axially Aligned Threaded Joints

Sandro Alie Aldana, M.S.
University of Nebraska, 2021
Advisor: Keegan J. Moore

Maintaining effective preload in bolted joints is critical for ensuring long-term performance and safety throughout the operation of any assembled structure. The loosening of bolted joints has been studied since the Industrial Revolution, but modeling approaches have only emerged over the past three decades. Although existing approaches are capable of simulating or predicting loosening in a single joint consisting of a single bolt, they are too computationally expensive to be used to model loosening in large structures consisting of many bolts. The objective of this thesis is to construct and employ a reduced-order modeling (ROM) approach that treats the internal tension or the torque applied to the joint as a degree-of-freedom (DOF) that evolves dynamically with the structure. In this thesis, the approach is applied to threaded joints coupling axial rods and the torque applied to each joint treated as the new DOF. The method is first applied to predict the loss of torque in a system consisting of two axial rods connected by a single threaded joint and the simulated results are compared to experimental measurements. The method is then used to investigate the dynamic interactions between two threaded joints coupling three axial rods together. The idea is that by understanding these interactions, they can be exploited to nullify loosening or even heal joints that have already loosened. The results demonstrate that the behavior of the three-rod system can be divided into five regimes based on loading: first, a low-amplitude regime where each joint is independent of the other; second, a regime where

the joints exhibit weak dependence on each other; third, a regime of strong dependence; fourth, a regime where bands of mitigation arise corresponding to only one joint loosening; and fifth, a regime corresponding to complete rapid loosening of the first joint. The third and fourth regimes reveal that when the joints are torqued to the same initial preload, regardless of the actual value, both joints will always loosen. However, when the joints are tightened to different amounts, there exist combinations where only one joint loosens, such that the other joint maintains some of the initial preload.

Acknowledgements

This work was completed utilizing the Holland Computing Center of the University of Nebraska, which receives support from the Nebraska Research Initiative.

Table of Contents

List of Figures

List of Tables

CHAPTER 1- INTRODUCTION TO THE LOOSENING OF BOLTED JOINTS

1.1 Background

Industries such as automotive, aerospace, biomedical, defense, construction, and many others are all affected by the loosening of bolts in their structures. In all of these fields, structures typically contain dozens if not hundreds to thousands of bolted joints and the loss of preload in these joints can result in catastrophic failure. For example, an EQ-4B Global Hawk, one of the United States' most advanced and expensive unmanned aerial vehicles, lost stability and crashed in 2011 because a single screw loosened (Lozier 2012). The loosening of screws and bolts during operation often results in catastrophic failure, as evidenced by the 2013 Brétigny-sur-Orge train crash in Paris that resulted in seven deaths and 32 injuries, which was caused by the loosening of the bolts on the fishplate (rail joint) that connects the rails together (French Land Transport Accident Investigation Bureau 2015). Damage, injuries, and fatalities due to the loosening of bolted joints are not limited to such dramatic events. A 2017 survey of 103 public playgrounds by Olsen and Kennedy (2018,2020) found that 29.1% of playgrounds surveyed contained loose fasteners and presented a danger to children. In the health technology field, the Emergency Care Research Institute (2020) found that loosening of bolts cause so many injuries that they ranked among the top 10 health technology hazards in 2020. Furthermore, loosening of screws in biomedical implants is notoriously common: Becker and Becker (1995) reported that 43% of dental retaining screws loosen in the first year of service, and Wu et al. (2019) found that 33% of spinal screws loosen

within two years of service. Kaminskaya and Lipov (1990) reported that loosening of threaded fasteners causes 20% of all failures in machine tools and that the time to fix these failures is often on the order of 10% of the operating life of the machine. In the automotive industry, Holmes (1988) found that 23% of all automobile service issues resulted from loose bolts and that 12% of all new cars surveyed contained loose bolts. These metrics are reinforced by recent recalls due to loosening bolts, including 1.38 million Ford vehicles recalled in 2018 and fourteen recalls in 2021 alone as stated by the National Highway Traffic Safety and Administration (Ford Motor Company 2018; 2020; National Highway Traffic Safety and Administration 2020; 2021; NHTSA 2021).

To prevent these failures, a deeper understanding of both the mechanics of loosening and the interactions between multiple joints due their effect on the global dynamics of the structure is needed. Previous work has focused on understanding the mechanics of loosening using high-fidelity finite element models that try to create as close to real conditions as possible by including thread geometry and contact mechanics into the models. Although the results of such models are insightful, their high computational cost limits their applicability to simulating loosening in only a single joint containing one bolt, such that it is not possible to investigate interactions between multiple bolts and joints. The current way to model and simulate joints loosening is limited to a singular joint. In place of hyper-realistic modeling approaches, this thesis implements a recently developed reduced-order model (ROM) for loosening as investigated by (Moore et al. 2017) to investigate the interactions between multiple joints that arise due to the effect of the joints on the global dynamics of the structure.

1.2 Objective of the Present Research

The objective of this research is to determine how the loosening of one joint affects the behavior and evolution of a second joint in a system of three axial rods subjected to varying shock loads and coupled together using two axially aligned, threaded joints. Specifically, it is hypothesized that because the loosening of either joint alters the global dynamics of the system, the loosening of one joint will affect the behavior of the other joint and may even prevent the second joint from loosening. Confirmation of this hypothesis implies that it is possible to manipulate the design and behavior of bolted joints to passively mitigate loosening in some or all fasteners. Additionally, confirmation would also imply that one could incorporate dummy bolts that serve as a warning system by loosening prematurely and signaling the need for maintenance in the structure. Thus, the focus of this thesis is on testing this hypothesis using a computational model that incorporates a validated ROM for loosening in axially aligned, threaded joints.

1.3 Scope of this Thesis

This thesis is divided into 1) explaining the approach used to construct the proposed ROM and the validation of the ROM using previous experimental results; 2) the implementation of the ROM to model loosening of two joints in the system of three axial rods modeled using the spectral element method and associated convergence studies; and 3) an exploration of the behavior of the system with a focus on the interactions between the two joints based on their respective loss of torque and the analysis of the behavior using estimated total energies.

CHAPTER 2-LITERATURE REVIEW

2.1 Joint Loosening

Maintaining appropriate preload in bolted joints is critical for safe and efficient operation of nearly all built-up structures. Loss of preload during operation can be classified into two categories: non-rotational and rotational loss (Riveros, et al. 2016). The first category can further separated into embedding loss (local plastic deformation on the molecular scale), creep in gaskets (Nassar and Alkelani 2005; Nechache and Bouzid 2007; Alkelani, Housari, and Nassar 2008) or surface coatings (Yang Jun and DeWolf John T. 1999; Nah et al. 2012; Nah, Lee, and Choi 2014), stress relaxation (Tendo, Yamada, and Shimura 2000), thermal expansion (Sears and King 2004), wear of the threads or the clamped parts (Mingyuan Zhang et al. 2018; Ibrahim and Pettit 2005), and yielding caused by loading. Since the focus of this research is on the loss of tension caused by rotational loosening, non-rotational loosening will not be considered further in this thesis. The second category concerns the loss of preload that arises when the threads experience large relative rotations resulting in a release of the elastic energy stored in the joint. Moreover, this category is the most concerning as it can result in sudden and catastrophic failures during operation, and is widely recognized as one of the worst failure mechanism across many industries (Riveros, Mahmoud, and Rodriguez Lopez 2016).

Although loosening has been studied since the industrial revolution, our current understanding has only evolved over the past five decades. This understanding began with the seminal work by Junker (Junker 1969; 1972) where he showed that transverse motion, not axial motion, is the primary cause of rotational loosening in bolted joints. His

machine has since become the standard equipment for testing the self-loosening behavior of a single bolt (Junker 2008) However, because the machine applies the loading directly to the joint and does not mimic the dynamical behavior of the actual structure where the bolt will be used, the resulting measurements may not represent the actual behavior of the bolt during operation (Dominik 2015; Pichoff, Kummel, and Schiff 2018; Schiff 2019). The rotational loss of preload is dynamic and may occur over fractions of a second in the case of extreme shock loading (Foley et al. 2010; Dodson et al. 2012; 2014) or over relatively long periods of sustained vibrations (Junker 1969; 1972; Pai and Hess 2002a; Dinger and Friedrich 2011; Yokoyama et al. 2012). Note that the time periods considered in the latter case are still significantly shorter than those observed in non-rotational loosening. In his seminal works (Junker 1969; 1972), Junker demonstrated that the primary mechanism for rotational loosening was a sufficiently high shear force to induce slip of the bolt head. Further studies by Pai and Hess (2002a) demonstrated that loosening can occur even if the shear force is not large enough to cause the bolt head to slip. In this case, they determined that the loss of preload resulted from localized slip between the threads of the joint in addition to slip of the bolt head. Significant work was performed by Hess and his students (Hess and Davis 1996; Hess 1996; Hess and Sudhirkashyap 1997; Basava and Hess 1998) to investigate the effects of axial vibration on joint loosening and he introduced a reduced-order model (ROM) for axial joint loosening in his work (Hess and Sudhirkashyap 1997). This ROM is limited in that it assumes Coulomb friction and neglects transverse and bending motion of the bolt and effects of multiple threads. Additionally, the relative displacement across the joint is assumed to be a simple sinusoid with a constant frequency. Nassar and Housari (2005; 2006; 2007) introduced a

mathematical model and an accompanying experimental procedure to analytically model the loosening of a threaded joint subjected to transverse vibration. This work was later improved by Nassar and Yang (2009), who introduced integral equations for the cyclic shear forces and the bearing and thread friction torque components. Other approaches include investigations into the effects of interfacial pressure distributions on loosening, such as the work by Marshall, et al. (2010).

2.2 Current Modeling & Simulation

Dynamic modeling and prediction of self-loosening has only arisen in the past three decades through analytical methods and numerical studies using high-fidelity finite element models. On the analytical front, Hess and his students constructed a reduced-order model for the self-loosening under axial vibration by modeling the bolt threads as a free mass trapped between two inclines [45–48](Hess and Davis 1996; Hess 1996). The model was extended in (Hess and Sudhirkashyap 1996; 1997) to represent the dynamics of the entire bolt and used to study the effect of the location of a bolted joint in a cantilever beam (Rashquinha and Hess 1997). Zadoks and Yu (1997) showed that either slip at the threads or the bolt head is necessary for loosening, but neither are sufficient. However, they assumed that friction drops to zero once the bolt begins to slip, which has been shown to be an invalid assumption (Nassar and Housari 2006; Housari and Nassar 2007). Nassar and Yang (2007; 2008; 2009; Yang and Nassar 2011a; 2011b; 2013; Yang, Nassar, and Wu 2011) derived integral equations for different friction forces in a bolted joint and the bolt tension, Nassar and Abboud (2009) derived an improved stiffness for a bolted joint, and Yang et al. (2012) incorporated effects of plasticity into their models.

Fort et al. (2018; 2019) proposed a new criteria for self-loosening that relates the transverse deflection of the bolt to the relative transverse displacement across the joint.

With the rise of high-speed computing, many researchers have turned to the prominent finite element (FE) method for modeling loosening in the threaded joints. The effect of the rotation of the nut on bolt loosening was investigated by Shoji and Sawa (2005). They found that even if the nut rotates only a small amount each cycle, over many cycles, this summation of all rotations ultimately results in the complete loss of preload in the bolt.

Finite element models for studying the loosening of bolted joints typically require extremely fine meshes to accurately capture the thread geometry and contact conditions and only model an isolated bolted joint. Pai and Hess (2002b) developed one of the first FE models (6,126 nodes) and managed to reproduce different loosening motions observed experimentally. Jiang et al. (2003) incorporated both elastic and plastic effects, but the helical geometry of threads was excluded to simplify the problem. The FE models created by Izumi et al. (2007) (23,946 nodes) and by Zhang (22,387 nodes) (2006) improved upon these results, but the meshes were not fine enough to study local contact states. Dinger and Friedrich (2011) characterized the local slip states in the threads and bolt head during self-loosening using an FE model with 82,434 elements. Dinger later used a similar model with 167,900 elements to predict screw forming behavior (Dinger 2015). The effect of rotational and axial excitation have been investigated separately in (Yokoyama et al. 2012; J. Liu et al. 2017b) using models around 200,000 nodes. The effects of thread wear have also been predicted by Zhang et al. (2018; 2019) with models consisting of 80,546 and 432,529 nodes, respectively. Liu et al. (2019) managed to

predict the effects of self-loosening in a L-stub connection, but the model required 458,448 elements to accurately reproduce experimental measurements. Recently, studies on anti-loosening performance have been performed using models with around 500,000 elements in (Noda et al. 2016; Zhu, Hong, and Jiang 2016; Gong, Liu, and Ding 2018; Mo et al. 2020; Noda et al. 2020; Gong, Liu, and Ding 2021). Finally, Liu et al. (2021) studied the effects of torsional excitation on self-loosening using an FE model consisting of 1,385,142 elements. While these works and many others not cited often produce FE models capable of reproducing experimental observations, the FE models usually only capture the response of a single bolt. The reason is that, due to their geometry, the threads of a bolt are notoriously difficult to mesh and typically require extremely small elements, often introducing convergence issues in standard FE solvers. When convergence issues do not arise, the extremely low size of the elements results in a significant number of degrees-of-freedoms and, as a result, the simulations take considerable time. Consequently, high-fidelity simulations of bolt loosening in entire structures, which may possess dozens if not hundreds or thousands of joints, is simply not possible with current computing speeds.

Dynamic modeling and prediction of self-loosening has only arisen in the past three decades through analytical methods and numerical studies using high-fidelity finite element models. On the analytical front, Hess and his students constructed a reduced-order model for the self-loosening under axial vibration by modeling the bolt threads as a free mass trapped between two inclines (Hess and Davis 1996; Hess 1996). The model was extended in (Hess and Sudhirkashyap 1996; 1997) to represent the dynamics of the entire bolt and used to study the effect of the location of a bolted joint in a cantilever

beam (Rashquinha and Hess 1997). Zadoks and Yu (1997) showed that either slip at the threads or the bolt head is necessary for loosening, but neither are sufficient. However, they assumed that friction drops to zero once the bolt begins to slip, which has been shown to be an invalid assumption (Nassar and Housari 2006; Housari and Nassar 2007). Nassar and Yang (2007; 2008; 2009; Yang and Nassar 2011a; 2011b; 2013; Yang, Nassar, and Wu 2011) derived integral equations for different friction forces in a bolted joint and the bolt tension, Nassar and Abboud (2009) derived an improved stiffness for a bolted joint, and Yang et al. (2012) incorporated effects of plasticity into their models. Fort et al. (2018; 2019) proposed a new criteria for self-loosening that relates the transverse deflection of the bolt to the relative transverse displacement across the joint.

2.3 Background of the Proposed Modeling Approach

Given the cost of existing modeling methods, there is a need for reduced-order models (ROMs) that reproduce the dominant structural and dynamical effects of loosening joints at a fraction of the computational cost. This research develops a phenomenological ROM for the mechanics of loosening in bolted joints subjected to axial shock excitation. Specifically, the model introduces a mathematical relationship between the stiffness and torque of the joint and treats the torque as a new, dynamic internal variable governed by a first-order, ordinary differential equation. The model is applied to model the loosening of a threaded joint in a split-Hopkinson pressure bar (SHPB) (Hopkinson 1914; Kolsky 1949; Gray 2000; Chen and Song 2011) previously studied in (Moore et al. 2017) and others in (Foley et al. 2010; Dodson et al. 2012; 2014). In (Moore et al. 2017), the interface was modeled using an adjusted-Iwan element (Song et al. 2004), which

introduces a hysteric stiffness-displacement relationship to account for micro- and macro-slip of the joint and, consequently, incorporates nonlinear damping affects arising from friction. While this model was shown to reproduce the early-time response (i.e., before loosening occurs in the joint), it is unable to reproduce the loss of stiffness that arises during loosening of the joint at later times. As such, a primary goal of the present work is to reproduce the long-term dynamic response resulting from the loosening of the threaded joint.

CHAPTER 3-MODELING APPROACHES

3.1. Experimental Measurements and Results

3.1.1. Experimental Setup

This work considers the experimentally measured strain response of a split-Hopkinson pressure bar composed of two hardened AISI 1566 steel rods connected by a threaded interface (a representative schematic is presented in Figure 3.1) as discussed by (Dodson et al. 2014; Moore et al. 2017). The nominal material properties of the rods are $\rho = 7800$ kg/m^3, $E = 210$ GPa, and $\nu = 0.29$, and the length and diameter of each rod are 1.22 m and 0.038 m, respectively. The incident and transmission rods were machined with 1”-8 UNC male and female threads, respectively. Prior to the experimental measurements, the threaded interface is tightened using a DMC handle-less strap wrench (model BT-BS-618WT) and the resulting torque is measured 0.051 m from the interface using a Multitorq digital torque transducer (model 2503-F-MT) produced by CDI Torque Products. Following the tightening of the joint, a 0.152 m long striker is fired by a gas gun into the free end of the incident rod. The resulting impact introduces a transient stress wave into the incident rod, which propagates linearly through the incident rod until it is scattered nonlinearly by the threaded interface. The resulting strain waves were measured using semiconductor strain gages placed at two locations before (locations A and B) and two after the interface (C and D) and the analog measurements were conditioned using a Precision Filter 28000 chassis with a 28144A Quad-Channel Wideband Transducer Conditioner. The analog data were digitized using a National Instruments chassis and PXI-6133 multifunction input/output cards at a sampling rate of 2.5 MHz for a duration

of approximately 0.07s. Note that the strain gages were measured individually (without a Wheatstone bridge) and bending cancellation normally accomplished using a Wheatstone bridge (Chen and Song 2011) is performed during post-processing after the measurement. Following the measurement of the strain waves, the remaining torque in the interface was measured using the same torque transducer used to measure the torque prior to the striker impact. Additionally, the rotation of the joint was determined using a rotation index as shown in Figure 2. Further details of the experimental measurements can be found in (Dodson et al. 2014; Moore et al. 2017).

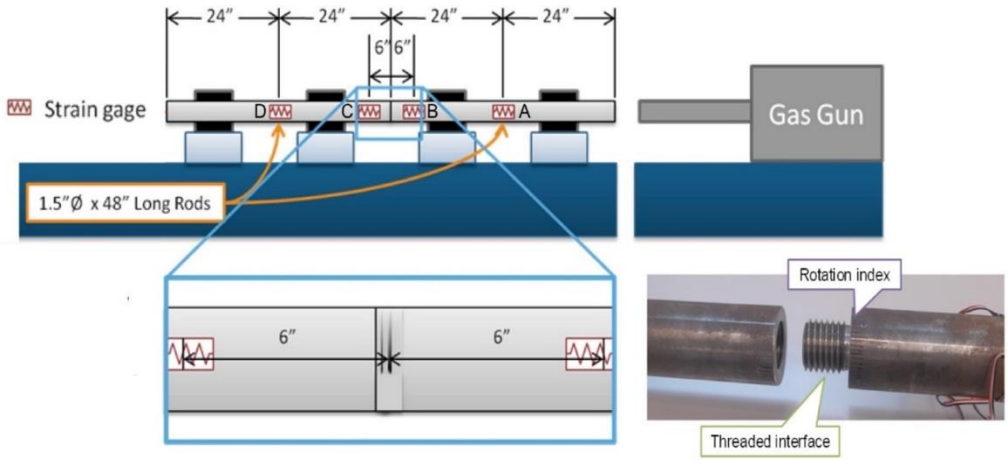

Figure 3.1 Schematic of the SHPB experiments showing the layout of the sensors and details of the threaded interface. Low-friction linear bearings support the system and both ends are free to move (modified with permission from (Dodson et al. 2014)).

3.1.2. Experiment Results

The response of the system was measured for combinations of five torque preloads (13.6, 30.5, 33.9, 41.5, and 54 Nm) and three impact velocities (7, 10.8, and 13.5 m/s). At each

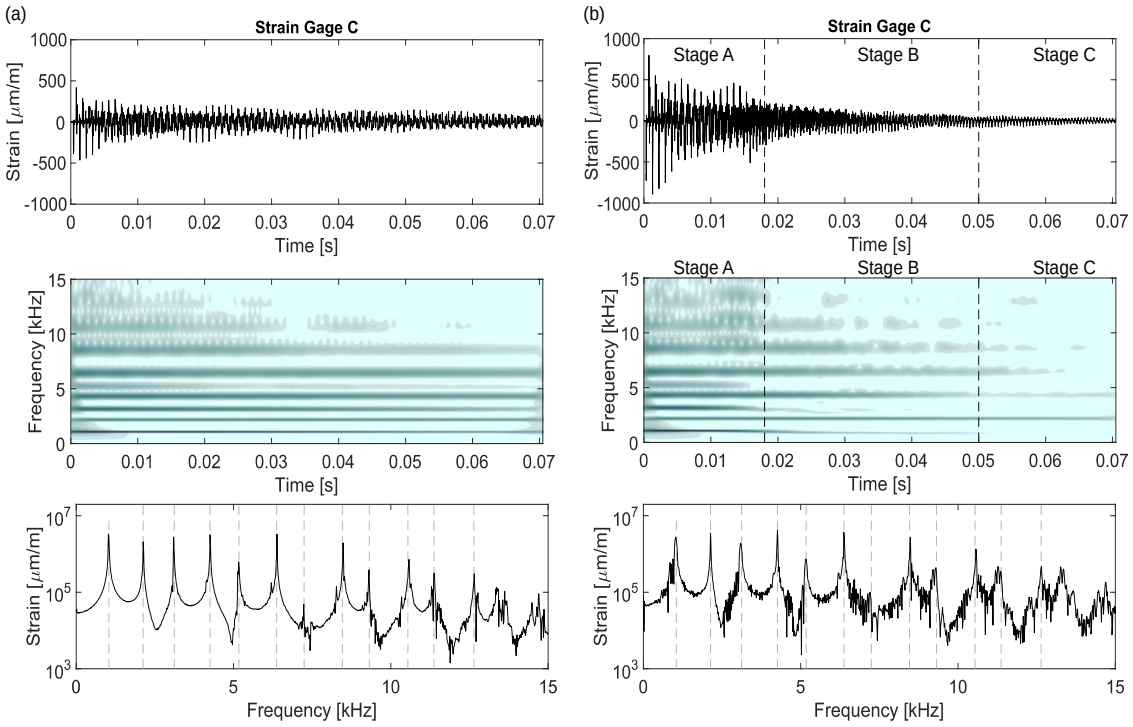

Figure 3.2 Longitudinal strain measurements, wavelet transform, and FFT at location C for torque preload of 54 Nm and impact velocities of (a) 7 m/s and (b) 13.5 m/s.

preload, at least three measurements were taken for each of the impact velocities, except for the case of a preload of 54 Nm and impact velocity of 13.5 m/s where just one measurement was realized due to the physical failure of the torque wrench. As discussed in (Moore et al. 2017), the response of the system is divided into three regimes based on the stored elastic energy in the joint (which corresponds to the input torque). First, at low torque, the joint is relatively loose, the coupling is weak, and the system behaves as if the two rods are not coupled at all. Second, for high torque, the joint acts as a rigid coupling between the two rods and the system behaves approximately as a single, linear rod. Finally, a strongly nonlinear transition regime connects the low- and high-torque regimes and all experiments discussed in this work measured the response of the system in this

regime. The reader is referred to (Moore et al. 2017) for further details regarding these regimes.

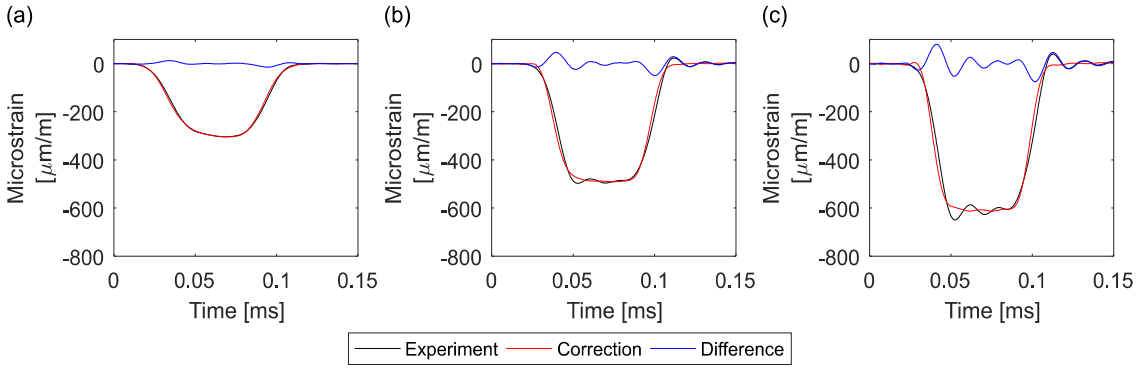

Figure 3.3 Dispersion-corrected incident pulse for impact velocities of (a) 7 m/s, (b) 10.8 m/s, and (c) 13.5 m/s. The black, red, and blue curves correspond to the experimentally measured pulses, the corrected pulses, and the difference of the experimentally measured pulses and the corrected pulses, respectively.

Due to the nonlinearity introduced by the joint, the response of the system not only depends on the stored elastic energy in the joint (i.e., the instantaneous torque), but also the type and amplitude of the excitation. More precisely, the dynamics are dependent on the total mechanical energy in the system and the energy content introduced by the excitation plays a vital role in the response of the system. To illustrate this dependence, Figure 3.2 compares the measured response of location C for a preload torque of 54 Nm and impact velocities of (a) 7 m/s and (b) 13.5 m/s. Comparing the time series of the two cases reveals a significant difference in dissipation rates and overall pattern of the response. Moreover, the increased dissipation in the second case (13.5 m/s) cannot be attributed to viscous damping alone and, thus, must arise from the loosening of the joint. Looking at the wavelet transform (WT) spectra, we find a drastic difference in the

harmonic content governing each of the responses (where lighter and darker shading correspond to low and high energy content, respectively). The WT of the first cast reveals that the response is primarily linear (at least up to 8 kHz) and this is confirmed by the fast Fourier transform (FFT) below the WT. In contrast, the WT (and the corresponding FFT) of the second case, show that the odd harmonics change significantly throughout the measurement, either abruptly exiting the dynamics or undergoing a significant reduction in frequency before exiting the response. Additionally, we find that the even harmonics are unaffected throughout the entire response, which implies that the joint only affects the odd harmonics. This is due to the geometry of the system; specifically, that the two rods are identical except for the threads. These effects can only be attributed to the significant nonlinearity introduced by the loosening of the joint. Except for a torque preload of 54 Nm and impact velocity of 7 m/s, the results of the second are reproduced in all other configurations of the system studied in this work. Furthermore, the response depicted in Figure 2(b) is divided into three different stages representing tight, loosening, and fully loose states of the joint. The reader is referred to (Moore et al. 2017) for further discussion of these stages.

Finally, the torsional motion induced by the loosening of the joint and the applied excitations were not measured in the original study. Since significant loosening and rotation was observed in the joint, there must be a conversion of axial waves to torsional waves. As pointed out by a reviewer of this work, the torsional waves must reverberate back and forth in an undoubtedly complex manner and could potentially contribute to the loosening of the joint. Moreover, it is hypothesized that the torsional waves interact parasitically with the axial waves; that is, the some of the energy carried by the axial

waves is irreversibly transformed into torsional waves. As such, the torsional waves represent an additional source of energy loss for the axial motion that is not accounted for in this work directly. However, this additional loss is approximately accounted for by the estimation of the linear damping parameters (which are likely overestimated due excluding this phenomenon). To investigate this hypothesis and the effects of torsional waves, future measurements of the torsional motion are necessary for this system or a similar one. The applied excitations are estimated from the incident pulses measured at location A. Since some dispersion was observed in the incident stress waves (Moore et al. 2017) these cannot be used directly as the excitation pulses. Instead, the incident pulses are numerically corrected for dispersion by phase-shifting each component of the FFT of the incident pulse as described by Gorham in (Gorham 1983). This method requires that the propagation velocities be known at each frequency and these were interpolated from the table provided by Bancroft in (Bancroft 1941). The representative incident pulse for each impact velocity are presented in Figure 3.3 (reproduced with permission from (Moore et al. 2017)), which shows that, after numerical correction, the incident pulses are approximately square. Thus, the numerically corrected impulses are representative of the actual impulses and will be used as inputs to the models of the system.

3.2. Finite Element Model

3.2.1. Linear Finite Element Model Identification

The rods are assumed to be continuous, homogeneous, and uniform with density of $\rho = 7800$ kg/m^3 and elastic modulus of $E = 210$ GPa. Each rod is modeled by discretizing

the linear, one-dimensional wave equation using the finite element (FE) method with 150 nodes, resulting in a total of 300 degrees of freedom. The resulting FE models for each rod (identical due to geometry and material) are coupled at the interface nodes using a linear elastic spring (to be replaced by the proposed model later). The stiffness of the spring corresponds to the initial stiffness of the joint. The initial stiffnesses of the joint were determined in (Moore et al. 2017) by matching the natural frequencies of the FE model with those measured experimentally in the early time response (before loosening occurs in the joint). This identification was accomplished by minimizing the error norm

$$\varepsilon_k = \frac{1}{6}\sum_{n=1}^{6}\frac{1}{2n+1}\left|\frac{\omega_{2n+1}^{exp}-\omega_{2n+1}^{FE}}{\omega_{2n+1}^{exp}}\right|, \tag{3.1}$$

using the *patternsearch* algorithm from the Global Optimization Toolbox for MATLAB® version 2020a.. The error norm e_k considers only the first six odd modes and is weighted such that the lower modes take precedence over the higher ones. Only the odd modes are considered because the even ones are entirely unaffected by the coupling between the two rods. Furthermore, the rigid-body mode that results from the free-free boundary conditions used in the FE model is neglected in the minimization as the joint stiffness has no effect on it and it does not appear in the strain measurements (as expected). The initial guess for the stiffness was set to 9.098×10^8 N/m, which is 10% of the stiffness of the interface region if it were a solid connection instead of a jointed connection. The default tolerances for *patternsearch* were used except for the mesh tolerance, which was set to 10^{-6} The resulting stiffnesses are independent of the excitation velocity (as expected) and are listed Table 3.1 for the five torque preloads considered.

Table 3.1 The identified interface stiffnesses for the five torque preloads measured

Torque Preload [Nm]	Identified Stiffness [GN/m]
13.6	4.12
30.5	6.41
33.9	7.07
41.5	7.73
54	8.53

The linear damping of the rods is modeled as viscous and proportional. While numerous methods exist for identifying viscous damping for linear response data (Silva 1999; Ewins 2000; Kim Saang Bum, Spencer B. F., and Yun Chung-Bang 2005), these typically require frequency-response functions constructed from the measured force and displacement or acceleration response. Due to the nature of the experiments, the input force can only be estimated numerically as described previously; however, no displacement or acceleration measurements were captured during the experiments and only the measured strains at the four locations are available to identify the linear damping of the system. As such, the damping is identified using a time-series optimization approach using the 54 Nm and 7 m/s cases (since this case corresponds to primarily linear response). First, the damping is assumed to be directly proportional to the mass and stiffness matrices of the uncoupled system, such that

$$D = \alpha M + bK, \tag{3.2}$$

where D is the damping matrix, K is the stiffness matrix, M is the mass matrix, and α and b are the proportionality constants to be determined with units of s^{-1} and s, respectively. The stiffness matrices without coupling are used to avoid introducing a

damping term that couples the two rods. Naturally, there must be damping in the joint that couples the two rods, but the objective of this work is to capture such effects using the proposed model and not the linear viscous damping. The values for a and b are identified by maximizing the R-squared value between the measured response and that predicted by the FE model simulation. Note that a similar approach was employed in (Kurt et al. 2015; Moore et al. 2018; Bunyan et al. 2018) for coupled oscillators. Additionally, the optimization is constrained such that the maximum absolute amplitude of the last 20% of the predicted response $(0.0564 \pounds t \pounds 0.0705\,\text{s})$ is at least 80% and no more than 120% of the amplitude of the measured response in that same period. This constraint is added to prevent the estimated damping from being too large or too small (resulting in too much and too little dissipation, respectively). Due to this constraint, the objective function is non-smooth and gradient-based approaches cannot be used. Instead, the *patternsearch* algorithm in MATLAB®, which is a direct-search method, is used to maximize the R-squared value between the measured and predicted responses. The default tolerances are used and the initial guess is set to $a = 15\text{s}^{-1}$ and $b = 10^{-8}$ s. The optimization routine resulted in $a = 15.4196$ s^{-1} and $b = 2.0355 \times 10^{-8}$ s.

The accuracy of the identified FE model is verified by comparing the numerically predicted response with that measured experimentally. Specifically, Figure 3.4(a) presents the comparison for the 54 Nm and 7 m/s case, which was used in the identification. The time series show that the FE model prediction agrees well with the measured response and that the identified damping model is reasonable. Furthermore, the WT spectra also show strong agreements between the model and the experiment. The

worst agreement occurs in the fifth mode, which indicates that the damping is too low for this mode. The strong agreement in the WT spectra is also observed in the corresponding FFTs. Overall, the identified FE model is able to reproduce the linear response.

However, the identified FE model is unable to reproduce the measured response whenever significant loosening occurs in the joint. For example, Figure 3.4(b) compares the measured response with that predicted by the linear FE model for a torque of 54 Nm and an impact velocity of 13.5 m/s. In this case, there is significant disagreement in not only the amplitude of the time series (corresponding to incorrect damping), but also in the overall pattern of the response (corresponding to the lack of loosening in the model). The WT spectra also reveal significant disagreement between the model and the experiment, which further highlights the nonlinear effects of the loosening joint. While the resonant peaks in the FFT of the predicted response are sharp and distinct, those of the experiment are blunt and indistinct. In fact, numerous peaks appear around the linear resonant peaks for the odd harmonics, further illustrating the nonlinear effects of the loosening joint.

We conclude this section by noting that even though the 54 Nm and 7 m/s case behaves linearly in the frequency range studied in Figure 3.4(a), the joint does undergo some loosening during the response. Indeed, Dodson et al reported in (Dodson et al. 2014) that the breaking torque of the joint after the measurement was approximately 20 Nm, resulting in a loss of around 63% of the initial torque. Despite such a large torque loss, the loosening of the ,joint in this case does not affect the first five odd harmonics of the response, which permits the identification of the linear FE model discussed previously.

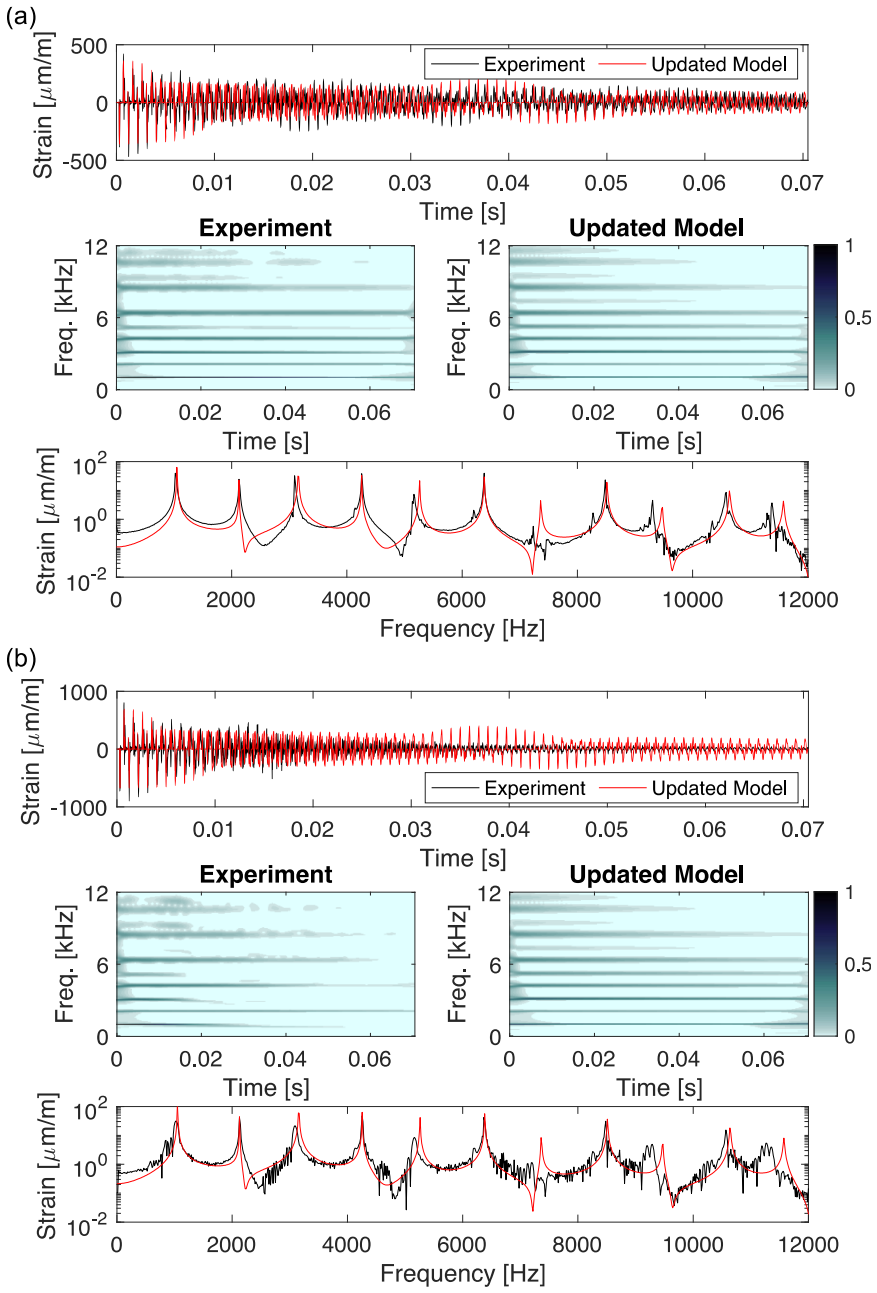

Figure 3.4 Comparison of the linear FE model with the experimental measurements. Specifically, a comparison of the time histories, WT, and FFTs of the longitudinal strain at location C for a preload torque of 54 Nm and velocities of (a) 7 m/s and (b) 13.5 m/s.

3.3. Modeling of the Bolted Joints

3.3.1. Proposed Modeling Approach

In this work, we investigate the loosening mechanics of bolted joints due to axial vibrations by considering a system composed of two elastic parts joined by a bolted joint and subjected to axial shock excitation. Although the threaded interface introduces both nonlinear stiffness and damping effects, the focus of this research is on a reduced-order model for the loss of stiffness that occurs as the joint loosens. As such, any nonlinear damping effects that arise due to sliding or slip of the threads in the joint are neglected and left open for future research. With this in mind, we consider the system presented in Figure 3.5 where the threaded interface is represented by a nonlinear force that depends on the relative displacement across the interface, $z(t)$, which is defined as

$$z(t) = u_2(0,t) - u_1(L,t). \tag{3.3}$$

Since the axial stiffness obviously depends on the torque applied to the bolt, we model the interface force using a nonlinear stiffness coefficient that depends on the torque multiplied by the relative displacement across the interface.

A suitable form for $k(T)$ can be determined based on some physical observations. First, if the joint is in a low-torque state then increasing the torque should result in a larger increase in stiffness than if the joint is in a high-torque state (i.e., diminishing returns). The physical reasoning is that, when the joint is relatively loose, friction is weak and the majority of the work done on the joint results in an increase of stiffness. In contrast, when the joint is tight, friction is strong, the majority of the work is spent overcoming friction, and only a minority actually increases the stiffness of the joint. As

such, for any torque-stiffness model to be physically representative of a threaded joint, its slope must be large near the origin and small at large torques. Furthermore, there is an upper limit that the stiffness of the joint can achieve, and this is equivalent to the axial stiffness of a solid rod of equivalent dimensions and material as the joint, which we represent as k_a. The value of k_a depends on the geometry and material of the joint and can be calculated using basic linear elasticity theory. In reality, this stiffness is only realized if the applied force on the joint is so large that the components cold weld and become inseparable. Mathematically, these observations are

$$\frac{dk}{dT} > 0 \text{ as } T \to 0, \tag{3.4}$$

and

$$\frac{dk}{dT} \to 0 \text{ as } T \to T_m, \tag{3.5}$$

where T_m is the maximum possible torque at which the stiffness of the joint is equal to the theoretical maximum stiffness, k_a, described previously. Note that for $T > T_m, k(T) = k_a$.

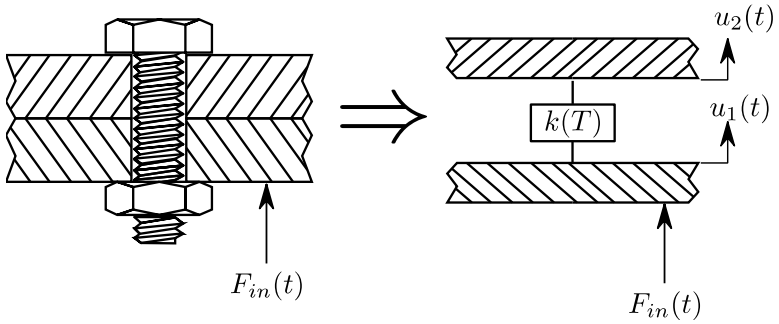

Figure 3.5 The proposed model for the stiffness of the bolted joint

One model that can capture these observations is

$$k(T) = k_a \left[1 - \left(1 - \left(\frac{T}{T_m} \right)^{\alpha} \right)^{\beta} \right], \tag{3.6}$$

where $k(T_m) = k_a$ and the dimensionless parameters α and β control the shape of the curve near the origin and T_m respectively. Taking the first derivative of Equation 3.6 results in

$$\frac{dk}{dT} = \frac{\alpha\beta k_a}{T_m} \left(\frac{T}{T_m} \right)^{\alpha-1} \left(1 - \left(\frac{T}{T_m} \right)^{\alpha} \right)^{\beta-1}. \tag{3.7}$$

Then for $T \to 0$,

$$\frac{dk}{dT} \to \frac{\alpha\beta k_a}{T_m} \left(\frac{T}{T_m} \right)^{\alpha-1}, \tag{3.8}$$

and if $\alpha > 1$ then $\frac{dk}{dT} \to 0$. Thus, we require that $\alpha \leq 1$. For $T \to T_m$,

$$\frac{dk}{dT} \to \frac{\alpha\beta k_a}{T_m} \left(1 - \left(\frac{T}{T_m} \right)^{\alpha} \right)^{\beta-1}. \tag{3.9}$$

If $\beta < 1$then $\frac{dk}{dT} \to \infty$ and if $\beta = 1$, then $\frac{dk}{dT} \to \alpha k_a T_m^{-1} \neq 0$. Thus, we find that

$$\alpha \leq 1 \text{ and } \beta > 1. \tag{3.10}$$

As will be discussed in Section 3.3.2, values for $\alpha, \beta,$ and T_m can be determined directly from experimental measurements of the torque and estimates of the interface stiffness. Note that the value of T_m may be verified experimentally, but this is not possible without permanently bonding the interface.

Although the initial torque can be measured, under large enough excitation, the torque changes dynamically and may experience either a net loosening or net tightening effect (Hess and Davis 1996). In the case of net loosening, experiments described in

(Kasei 2007) showed that loosening occurs during loading of the joint and tightening occurs during unloading, with the loosening dominating the tightening to produce a net loss of torque. To reproduce the net loosening effect observed experimentally, the torque is modeled using a first-order, homogeneous ordinary differential equation (ODE):

$$\dot{T} + f(T) = 0. \tag{3.11}$$

Note that the ODE governing the torque is homogeneous because there should be no external influence operating on it. In other words, no external work is done on the joint to increase or decrease the torque. A functional form for $f(T)$ can be determined by recognizing that the torque will only change if there is significant relative motion in the interface. Thus, $f(T)$ must depend on the relative motion of the joint, or $f(T) = f(T, z, \dot{z})$, and a simple model that captures this is

$$f(T, z, \dot{z}) = q(z, \dot{z})T. \tag{3.12}$$

Further simplification comes from recognizing that the joint will not rotate when subjected to a monotonic tensile load. In such cases, any apparent loosening results from permanent plastic deformation of the joint and not rotation. Thus, the author hypothesizes that the rate of loss of torque due to rotation is dependent solely on the relative velocity of the interface, giving $f(T) = q(\dot{z})T$ Furthermore, since the model is intended to reproduce only a net loosening effect, the rate of loss of torque, $q(\dot{z})$, must be independent of the sign of the relative velocity. A simple model that satisfies these conditions is

$$f(T) = \gamma \dot{z}^2 T, \tag{3.13}$$

where γ is a constant that scales the rate of loss of torque and the resulting ODE is

$$\dot{T} + \gamma \dot{z}^2 T = 0, \tag{3.14}$$

Equation 3.14 which is a linear, homogeneous, first-order ODE, with the following solution

$$T(t) = T(0) \exp\left[-\gamma \int_0^t \dot{z}^2 d\tau\right], \tag{3.15}$$

which implies that $\mathcal{G}$ could be directly determined from experimental measurements of the interface velocity and the instantaneous torque in the joint.

3.3.2. Identification of Parameters of the Proposed Model

With the linear FE model identified and validated, we now proceed with the identification of the parameters of the proposed model (α, β, T_m, and γ). We start with the identification of α, β, and T_m which correspond to the proposed torque-stiffness relationship

$$k(T) = k_a \left[1 - \left(1 - \left(\frac{T}{T_m}\right)^{\alpha}\right)^{\beta}\right], \tag{3.16}$$

where $T_m$is the maximum torque possible at which $k(T_m) = k_a$, k_a is the maximum possible stiffness (i.e., the stiffness of the joint if it were a solid connection instead of jointed), and α and β control the curvature near the origin and T_m, respectively. As discussed previously, the identification of these parameters relies on knowing the stiffness of the joint prior to loosening and the corresponding torque preload. The stiffness for the five preloads considered in this work were identified in (Moore et al. 2017) (briefly discussed in the previous section) and are provided in Table 3.1. Using these values, the unknown parameters governing the torque-stiffness relationship are identified by employing a curve-fitting procedure to maximize the R-squared value between the data from the experiments and the predicted model. This identification was performed using *patternsearch* with default tolerances except for the mesh tolerance,

maximum iterations, maximum number of function evaluations, and the termination tolerance on the function value, which were set to 10^{-12}, 10^{6}, 10^{6}, 10^{-12}, and 10^{-12}, respectively. The initial guesses, lower bounds, upper bounds, and the identified values are presented in Table 3.2.

Table 3.2 The initial guess, lower and upper bounds, and identified values for α, β and T_m

Parameter	Initial Guess	Lower Bound	Upper Bound	Identified Value
α	0.5	0	1	0.7635
β	1.5	1	10	1.9543
T_m [Nm]	60	54	200	77.418

The resulting model is presented in Figure 3.6 and the R-squared value is 0.9999, indicating a near perfect agreement between the model and the data. This near perfect agreement results from the fact that only five data points are used to identify the model. Note that the lower and upper bounds reflect the limitations placed on $\alpha$and β, and that the lower bound for T_m is set to the highest torque preload obtained in the experiments. The initial guesses and the upper bounds of β and T_m were chosen arbitrarily. Note that one benefit of *patternsearch* is that it is insensitive to initial guesses so long as the tolerances are adjusted to allow *patternsearch* to explore the entire domain of the problem. With the torque-stiffness model identified, the FE model is updated such that the interface coupling is entirely governed by the identified model. We will refer to this model as the "updated FE model" in the upcoming discussion.

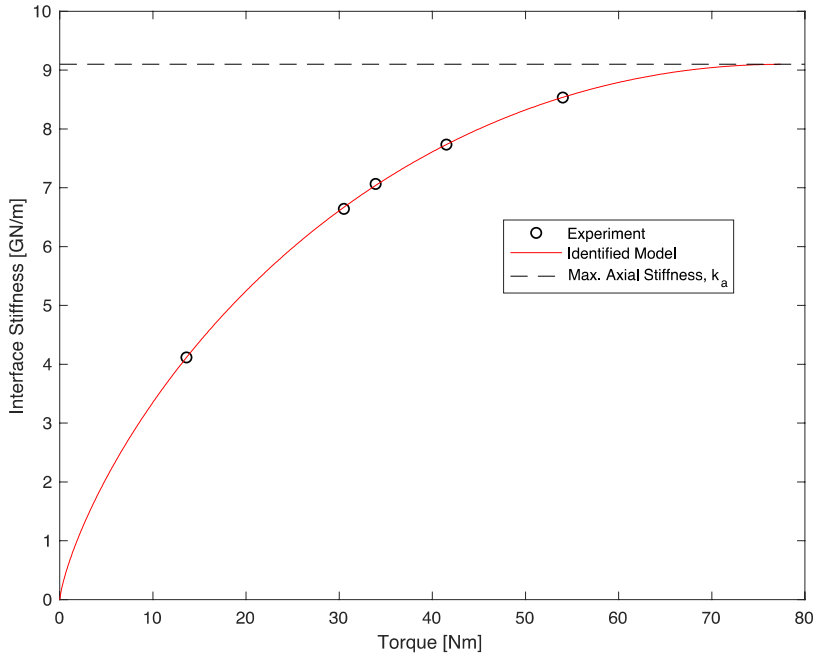

Figure 3.6 Comparison of the identified torque-stiffness ROM with the experimentally measured torques and identified interface stiffnesses. The upper limit of the axial joint stiffness is represented by the dashed, black line.

With the first three parameters identified, we now focus on the identification of γ, which controls the rate at which torque is lost in the joint. Recall from the discussion in Section 3.3.1, that the torque in the joint is modelled using the following first-order ODE

$$\dot{T} + \gamma \dot{z}^2 T = 0, T(0) = T_0, \tag{3.17}$$

where $\dot{z}$ is the relative velocity across the interface and T_0 is the torque preload applied to the joint. As described in Section 3.3.1, the value of γ can be directly identified from experimental measurement of the torque in the joint and the interface velocity, which can prove challenging for a typical bolted joint. For the axial joint studied, a reviewer suggested that, at least theoretically, the instantaneous torque and interface velocity could be obtained by applying a wave-separation method to the measured time series provided that the torsional motion is also measured. However, the torsional motion was not

measured in the original study (Dodson et al. 2014) and, instead, we identify γ by recognizing that complete loosening corresponds to the loss of half of the harmonics participating in the response. This loss is captured by the WT of the measured strain responses and, more importantly, by the IMA of the WT for the frequency range considered in this work. Thus, we identify γ by employing the procedure described in Section 3.2.1, where the R-squared value between the IMA of the WT of the experimental measurements is predicted by the updated FE model. Note that this procedure numerically integrates the updated FE model and Equation 3.17 for each value of γ. Given that γ is proposed as a scaling constant, it should be a joint-specific property that is independent of the impact velocity and the torque preload (this assumption will be evaluated in the next section). As such, the identification is performed using only the response from the first measurement of a torque preload of 54 Nm and an impact velocity of 10.8 m/s. Again, *patternsearch* was employed to perform the identification and default tolerances were used. The initial guess, lower bound, and upper bound were set to 2,400 , 0, and 10^4 s/m^2, which were determined based on initial simulations of the updated FE model. The procedure resulted in an identified value of $\gamma = 2{,}695.2$ s/m^2 and a corresponding R-squared value of 0.9453, indicating a strong agreement between the model and the experiment. The WT and the corresponding IMA of the measured and predicted strain responses at location C are presented in Figures 3.7(a) and (b), respectively. Figure 3.7(c) presents a comparison of the IMA of the WT of the measured and predicted strain responses at location C. The strong agreement observed in the WTs and the IMAs verifies the accuracy of the procedures employed to identify the unknown

parameters of the proposed model for the joint. We will refer to the final model, containing the linear FE model and the identified proposed model, as the "identified model" from here on.

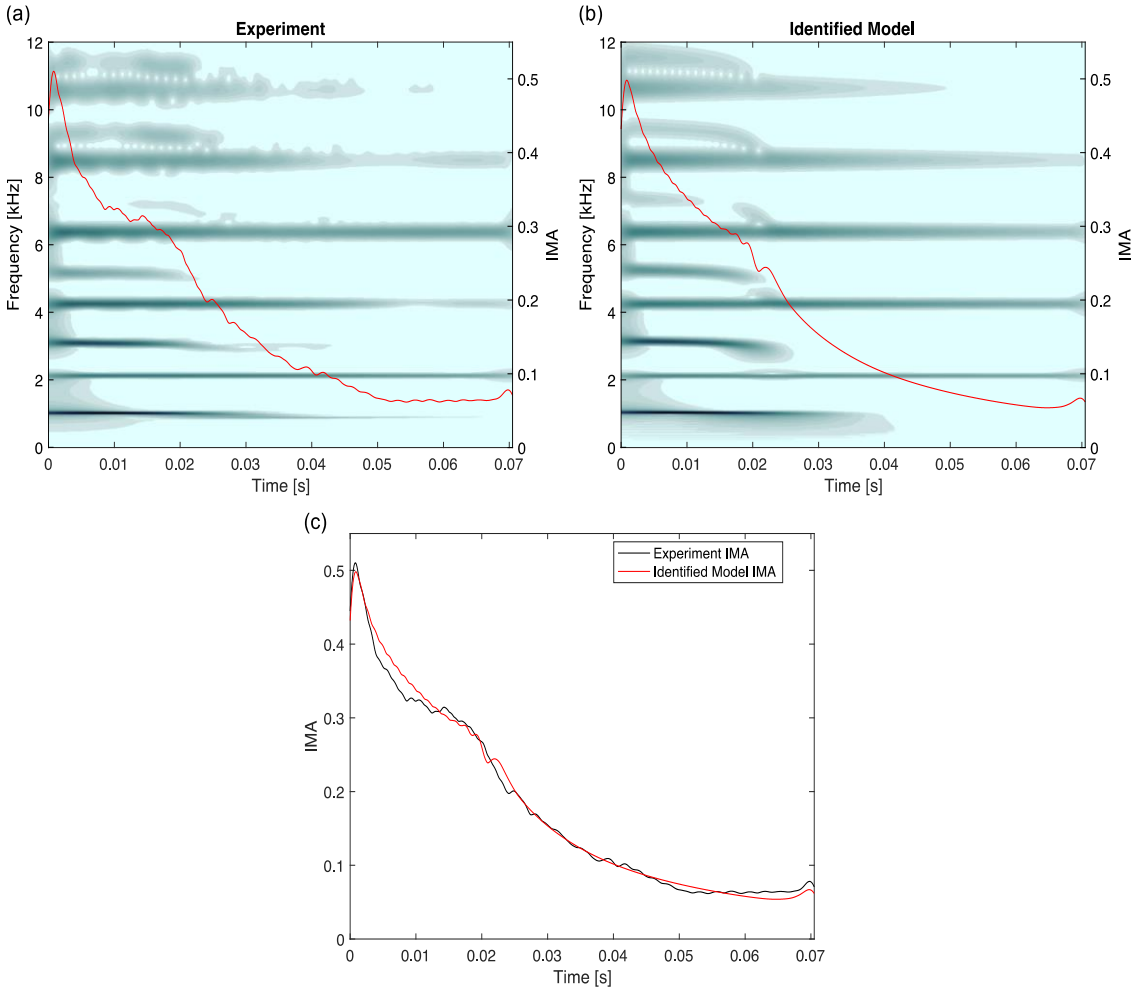

Figure 3.7 The WT of the strain at location C and the corresponding IMA for (a) the experiment and (b) the identified model. (c) Comparison of the IMA of the WT for the experiment and identified model.

3.4. Model Validation

To validate the identified model for the joint, we focus on comparing the numerical predictions with the experimental measurements for multiple torque preloads and impact velocities. First, we consider the case of 54 Nm torque preload and 10.8 m/s impact velocity (the case used for the identification of γ) and plot the measured and predicted time series, WTs, and FFTs of the strain response at location C in Figure 3.8. The comparison of the time series shows that both the dissipation and overall pattern of the measured response is reproduced by the identified model. This agreement indicates that the proposed model does capture the dominant effects of the loosening joint including both the loss of stiffness and additional dissipation. The comparison of the WTs shows further agreement between the experiment and the model. In particular, we note that the odd harmonics exit the predicted response at a similar time as they do in the experimental response. Moreover, the first four even harmonics persist throughout the entire response, which indicates that the proposed model does not influence them and that the identified damping is reasonable. Note that both of the WTs are normalized such that they appear on the same scale from 0 to 1, which was accomplished by dividing the amplitudes of both WTs by the largest amplitude between the two. Overall agreement is observed in the comparison of the FFTs; however, the predicted FFT deviates from the experiment FFT below the first odd harmonic. This disagreement occurs because the proposed model completely decouples the two rods when the torque is equal to zero (i.e., the interface stiffness is exactly zero when the torque is zero in the model). Naturally, there must be some weak, but non-zero, coupling between the two rods when the torque is zero in the

experimental system, which arises from the contact between the threads. The additional stiffness corresponding to zero torque in the joint is not considered in this work. The instantaneous torque in the joint predicted by the model is presented as the dark gray curve in Figure 3.9(a), and we find that the predicted torque rapidly decreases and appears to reach zero torque at approximately 0.022s. However, the torque appears to reach zero at this time due to the linear scale of the figure. Plotting the instantaneous torque on a logscale (the dark gray curve in Figure 3.9(b)) reveals that the torque continues to decay well past 0.022 s. For reference, when the torque in the joint is 0.1 Nm, the predicted stiffness of the joint is $1.1\acute{}\ 10^{8}$ N/m, which is large enough that the odd harmonics still participate in the response.

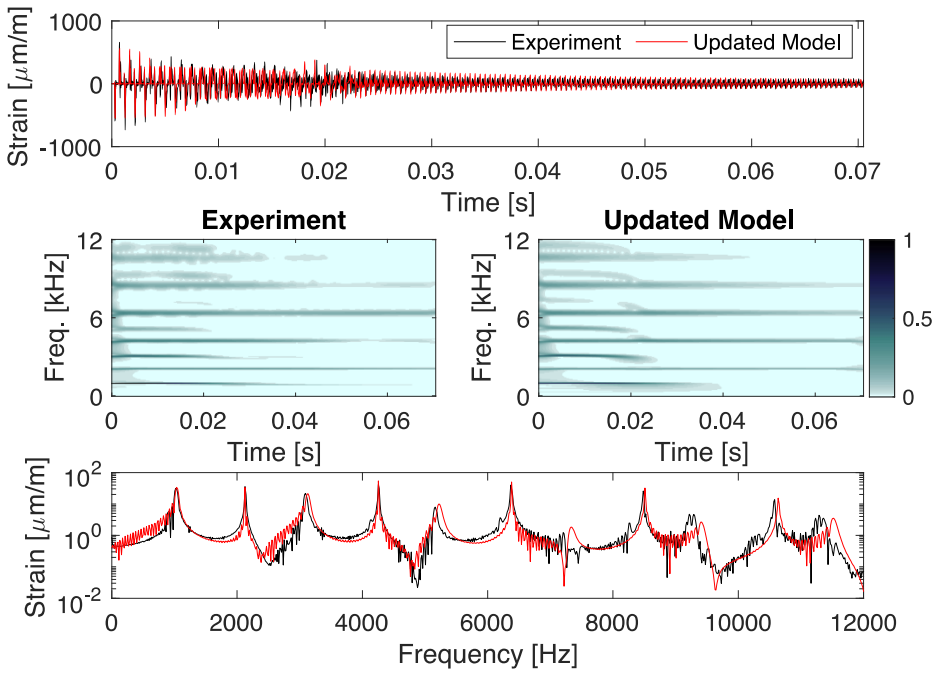

Figure 3.8 Comparison of the time series, WT spectra, and FFTs of measured and predicted strain responses at location C for impact velocity of 10.8 m/s and torque preload 54 Nm

While the previous comparison does validate the identified model, a stronger validation comes from applying the identified model to measurement cases not used in the identification of the joint parameters. First, we consider the case of a torque preload of 54 Nm and an impact velocity of 7 m/s, which was the case used to identify the linear viscous damping model for the rods earlier. Since this response was reproduced by the linear FE model, the resulting prediction from the identified model should also be linear and not deviate strongly from the predictions of the linear FE model. Figure 3.10 presents the time series, WTs, and FFTs for the responses measured experimentally and predicted numerically using the identified model. Comparison of the time series show strong agreement between the numerical prediction and the measured response in both the pattern of the response and the dissipation. This agreement is reflected in the WTs where none of the odd harmonics except the eleventh exit the response before the final measurement time. Finally, the FFTs also show agreement between the measured and predicted responses, and both responses appear linear below 9000 Hz. This indicates that either no loosening occurs in the joint at this torque preload and impact velocity or the loss of torque induced by loosening is too low to affect the lower harmonics of the system. Indeed, looking at the instantaneous torque predicted by the model (depicted as the black curves in Figures 3.9(a) and (b)), we find that the joint does indeed loosen, but total loss of torque is not realized as in the previous case (the dark gray curves in Figures 3.9(a) and (b)). Instead, the torque decays gradually throughout the response and approaches a constant level indicating the end of loosening in the joint. Overall, the identified model predicts that 61.1% of the initial torque preload is lost (approximately 33

Nm), which agrees well with the experimentally observed loss of 63% of the initial torque preload (approximately 34 Nm) (Dodson et al. 2014). The predicted loss of torque was determined by simulating the identified model for 0.5 s and the strain predictions from this simulation are omitted for brevity.

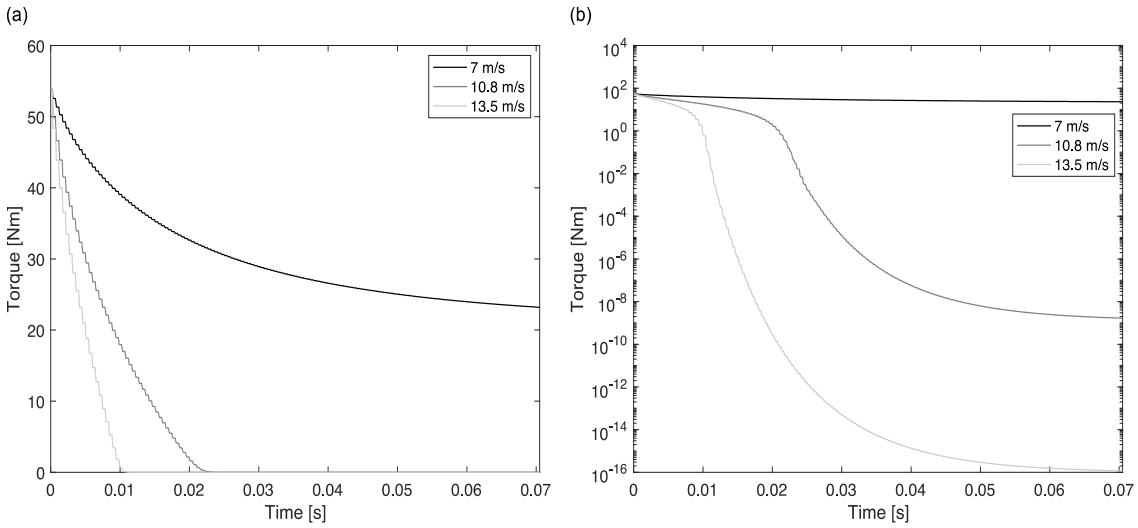

Figure 3.9 Comparison of the predicted instantaneous torques for a torque preload of 54 Nm plotted on (a) linear scale and (b) logscale.

As a second validation, we consider the case of a preload torque of 54 Nm and an impact velocity of 13.5 m/s, the highest impact velocity studied and the resulting time series, WTs, and FFTs are presented in Figure 3.11. From the comparison of the time series, we see that the identified model is able to capture the overall pattern and dissipation of the response. However, there is some small disagreement in amplitude between 0.01 and 0.02 s, which hints that the model slightly overpredicts the rate of loosening of the joint. This disagreement indicates that γ is a little too large for this specific measurement case, which hints that the assumption that γ is independent of the impact velocity is incorrect. Nevertheless, the strong correlation between the model and

the experiment implies that the proposed model serves as a suitable as a reduced-order model for the mechanics of loosening axial joints. Another disagreement appears in the amplitude of the predicted response towards the end of the response. Specifically, the predicated amplitude is larger than that of the experimentally measured response, which points to a disagreement between the dissipation in the identified and actual systems. This disagreement is expected because the proposed model does not incorporate any frictional effects and, thus, does not account for all sources of dissipation. However, the strong agreement in the overall pattern of the response indicates that the majority of the dissipation is captured using linear viscous damping and the identified model for the joint stiffness. Note that, since the loss of stiffness is dynamic and occurs when the displacement across the interface is non-zero, it is hysteretic and introduces additional dissipation into the model. Thus, the strong agreement between the time series indicates that the proposed model captures the majority of the energy dissipated by the joint. Comparison of the WTs shows that, despite predicting that complete loss of stiffness occurs at a slightly earlier time than in the experiment, the identified model reproduces the dominant effects of loosening in the joint. The agreement is also observed in the FFTs except for the frequency content below the first harmonic, but, as explained earlier, the model is not intended to capture the stiffness introduced by loose contact of the threads in the joint. The resulting instantaneous torque predicted by the model is depicted as the light gray curves in Figures 3.9(a) and (b), which shows the rapid loss of torque that occurs compared to the other two cases considered.

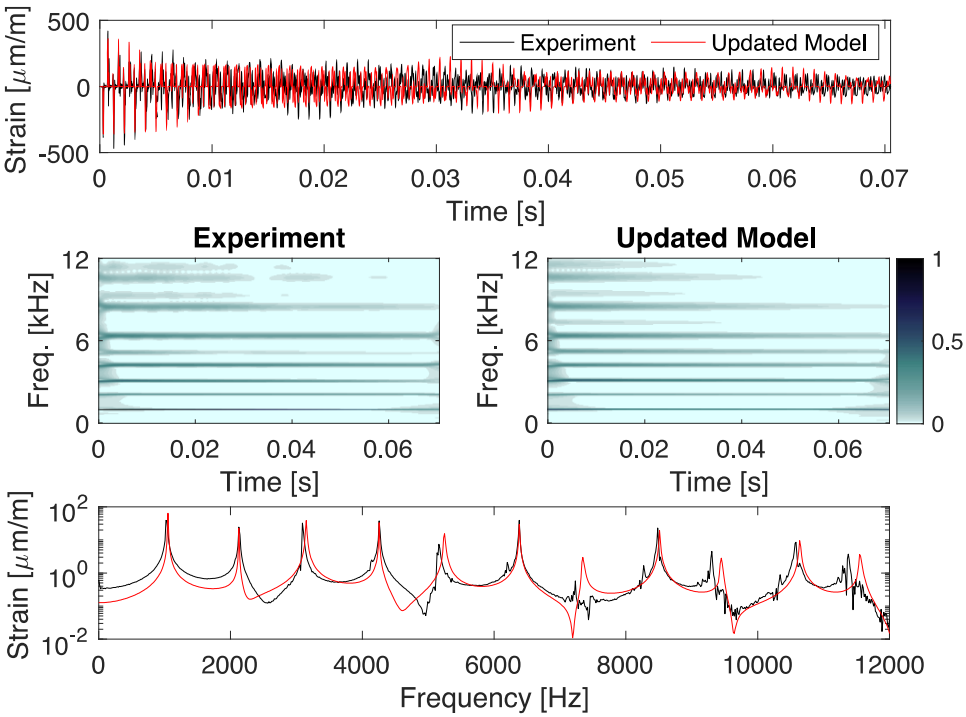

Figure 3.10 Comparison of the time series, WT spectra, and FFTs of measured and predicted strain responses at location C for impact velocity of 7 m/s and torque preload 54 Nm

To investigate the assumption that γ is independent of the initial torque preload, we apply the identified model to predict the strain response at a location C for an impact velocity of 10.8 m/s and torque preloads of 14 Nm and 34 Nm. The predicted and measured time series, WT spectra, and FFTs are presented for torque preloads of 14 Nm and 34 Nm in Figures 3.12(a) and (b), respectively. Comparing the responses for a torque preload of 14 Nm, we find that the identified model reproduces the overall pattern and dissipation profile of the measured response. However, there is some difference at early times, which indicates that there is a disagreement between the model and experiment in rate of loosening in the joint. Indeed, comparing the WT spectra, the loosening of the joint occurs more rapidly in the identified system than in the actual system. Comparison

of the responses for the 34 Nm case show that the rate of joint loosening is also slightly higher in the model than in the experiment, but the overall response is reproduced by the identified model. Based on the observations of these two cases, we conclude that the assumption that g is independent (or at most weakly dependent) of the torque preload and that the identified model is suitable for predicting the response of the system at torque preloads and impact velocities that are not directly used in the identification.

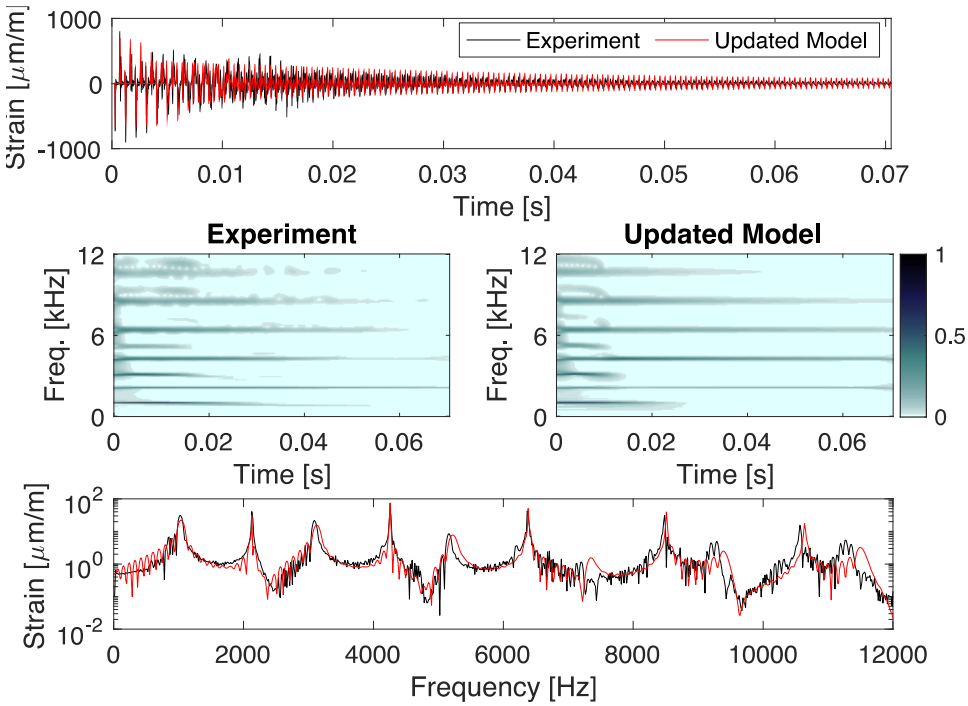

Figure 3.11 Comparison of the time series, WT spectra, and FFTs of measured and predicted strain responses at location C for impact velocity of 13.5 m/s and torque preload 54 Nm

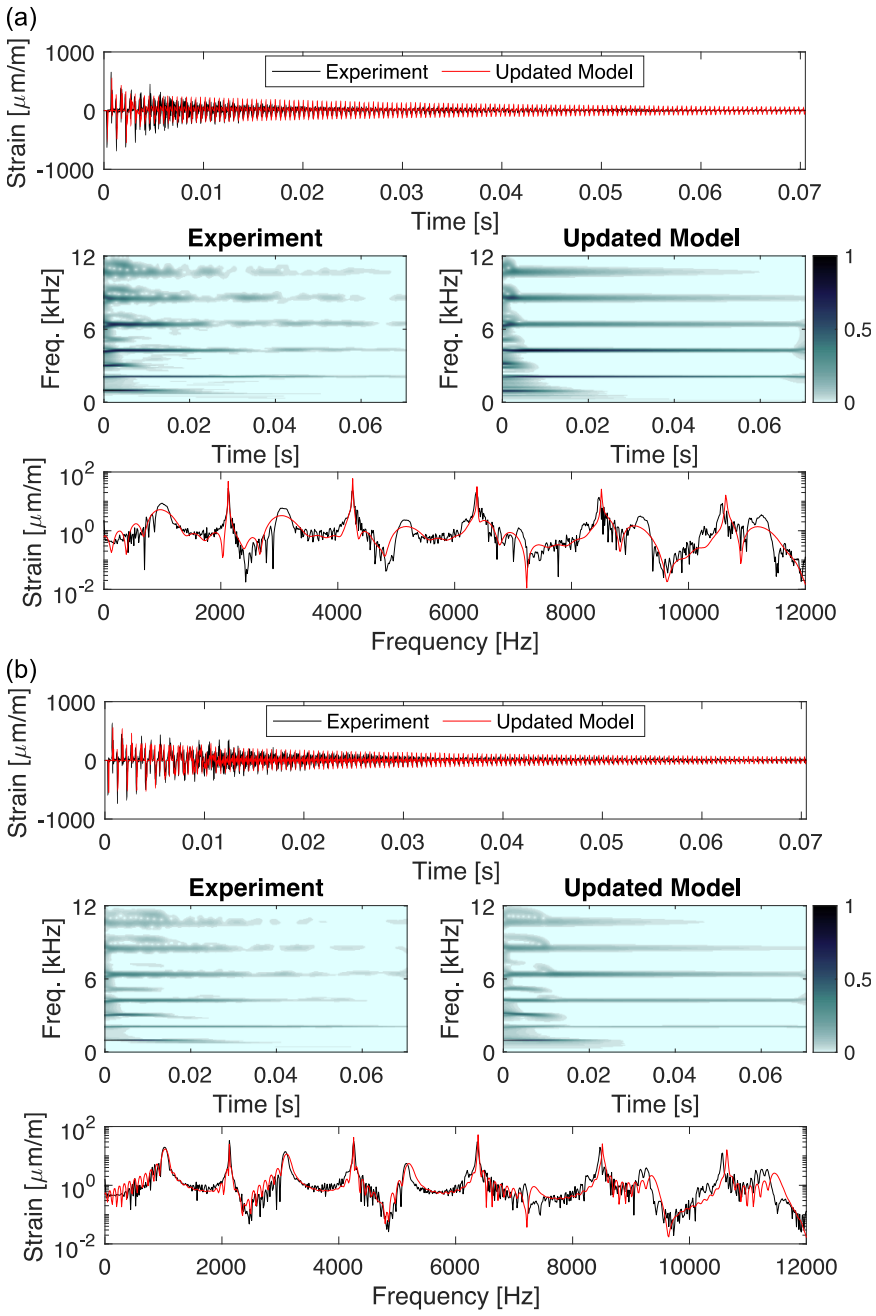

Figure 3.12 Comparison of the time series, WT spectra, and FFTs of measured and predicted strain responses at location C for impact velocity of 10.8 m/s and torque preloads of (a) 14 Nm and (b) 34 Nm

CHAPTER 4. DYNAMICS OF A MULTI-JOINTED SYSTEM OF THREE AXIAL RODS

This chapter concerns the dynamical behavior of a system composed of three identical axial rods coupled together using two axially aligned threaded joints. The theoretical system and its governing equations of motion are first presented and discussed followed by an investigation of the effect of the torque in each joint on the natural frequencies and mode shapes of the assembled system. This is followed by a preliminary investigation of the effect of loosening in one joint on the evolution of the other joint before performing a thorough analysis of the behavior of the system throughout different regimes based on the applied force.

4.1. The Theoretical System and Computational Model

The system investigated in this research is composed of three identical axial rods coupled together using two axially aligned threaded joints. The system is similar to the system studied in Chapter 3, except that a second joint and third rod are added to the previous system. A schematic of the system is presented in Figure 4.1 where the dynamics of the joints are represented by two nonlinear springs with stiffness that depends on the instantaneous torque in their respective joints. The instantaneous displacement of each rod is $u_i(x,t), i = 1,2,3$ and the rods are assumed to have a length of $L = 1.22$ m, diameter of 0.038 m resulting in an area of $A = 0.00113$ m^2, an elastic modulus of $E = 210 \times 10^9$ Pa, and a density of $\rho = 7800$ kg/m^3. Employing the proposed reduced-order modeling approach discussed in Chapter 3, the dynamics of the threaded joints are represented using linear springs with torque-dependent stiffness and are defined as

$$K_1\big(T_1(\dot{z}_1,t)\big) = k_a\left(1-\left(1-\left(\frac{T_1(\dot{z}_1,t)}{T_m}\right)^{\alpha}\right)\beta\right), \tag{4.1}$$

for the first joint and

$$K_2\big(T_2(\dot{z}_2,t)\big) = k_a\left(1-\left(1-\left(\frac{T_2(\dot{z}_2,t)}{T_m}\right)^{\alpha}\right)\beta\right), \tag{4.2}$$

for second joint. Here $T_1(\dot{z}_1,t)$ and $T_2(\dot{z}_2,t)$ are the instantaneous torques in first and second joint, respectively, $z_1(t) = u_2(0,t) - u_1(L,t)$ is the relative displacement across the first and second rods, $z_2(t) = u_3(0,t) - u_2(L,t)$ is the relative displacement across the second and third rods, $\alpha = 0.7635$, $\beta = 1.9543$, and $T_m = 77.418$ Nm. Note that the same model and parameters are used to model the torque-dependent stiffness of each joint. Although in practice every joint will differ slightly from another, the focus of this research is on how multiple joints can interact with each other through the global dynamics of the structure during loosening. Thus, using the same parameters for each joint eliminates the possibility that any observed interactions result from differences in parameters.

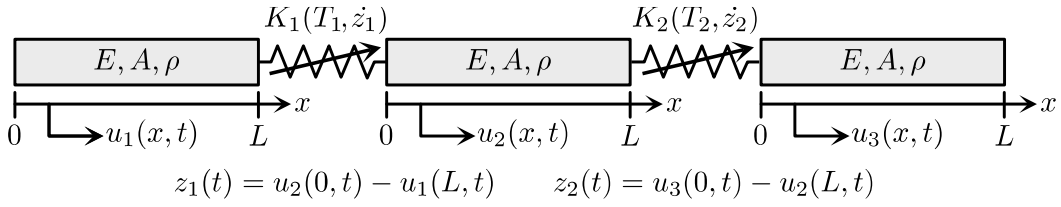

Figure 4.1 Schematic of the theoretical system consisting of three axial rods coupled by two axially aligned, threaded joints. The joints are modeled using the proposed reduced-order model and represented by nonlinear springs with stiffnesses that depend on the instantaneous torque in the joint and the relative velocity across the interface.

4.2. Spectral Element Model and Convergence Study

Each rod is modeled using the spectral element method (SEM) (Fichtner 2011) with 10 elements with Gauss-Labatto-Legendre (GLL) nodes corresponding to a Lagrange polynomial of degree 6 (Ampuero 2021). The appropriate number of elements was determined using convergence study that compared the behavior of a single rod meshed using 5, 10, 20, 50, and 100 elements with 31, 61, 121, 301, and 601 GLL nodes, respectively. The convergence study is performed by first comparing the natural frequencies of each model, by comparing the velocity response of the rod to an externally applied impulsive force, and by comparing the chosen SE model response with that predicted by the FE model used in Chapter 3.

The first part of the convergence study considers the natural frequencies for each model, and these are presented in Table 4.1 for the first 31 modes. The first 31 modes are reported because the model with 5 elements has 31 degrees-of-freedom and, thus, only 31 linear modes of vibration. The model with 100 elements is used as the baseline for determining the accuracy of the other models and the relative percent error for the natural frequencies of each model is computed as

$$\varepsilon_n^m = 100\left(\frac{\omega_n^{100} - \omega_n^m}{\omega_n^{100}}\right)\%, n = 1,2,3, \dots, \tag{4.3}$$

where m represents the total number of elements (i.e., $m = 5,10,20, \text{or } 50$) for the nth mode. The percent errors are reported in Table 4.1 for only the five- and ten-element models because the first 31 natural frequencies of 20- and 50- element models match those of the 100-element model exactly.

Table 4.1 The natural frequencies of the first 31 modes for the different numbers of elements.

Mode No.	5 Elements		10 Elements		20	50	100
	Nat. Freq. [Hz]	Error [%]	Nat. Freq. [Hz]	Error [%]	Nat. Freq. [Hz]	Nat. Freq. [Hz]	Nat. Freq. [Hz]
1	0	0	0	0	0	0	0
2	2127.9	0	2127.9	0	2127.9	2127.9	2127.9
3	4255.9	0	4255.9	0	4255.9	4255.9	4255.9
4	6383.8	0	6383.8	0	6383.8	6383.8	6383.8
5	8511.7	0	8511.7	0	8511.7	8511.7	8511.7
6	10640	0	10640	0	10640	10640	10640
7	12768	0	12768	0	12768	12768	12768
8	14896	0	14896	0	14896	14896	14896
9	17023	0	17023	0	17023	17023	17023
10	19151	0	19151	0	19151	19151	19151
11	21271	0.04	21279	0	21279	21279	21279
12	23405	0.01	23407	0	23407	23407	23407
13	25527	0.03	25535	0	25535	25535	25535
14	27641	0.08	27663	0	27663	27663	27663
15	29725	0.22	29791	0	29791	29791	29791
16	32347	-1.34	31919	0	31919	31919	31919
17	33957	0.26	34047	0	34047	34047	34047
18	35860	0.87	36175	0	36175	36175	36175
19	37567	1.92	38302	0.00	38303	38303	38303
20	38848	3.92	40430	0.00	40431	40431	40431
21	39349	7.54	42543	0.04	42559	42559	42559
22	48295	-8.07	44684	0.01	44687	44687	44687
23	49078	-4.84	46809	0.01	46814	46814	46814
24	49905	-1.97	48933	0.02	48942	48942	48942
25	50501	1.11	51054	0.03	51070	51070	51070
26	92060	-73.05	53171	0.05	53198	53198	53198
27	92124	-66.51	55281	0.08	55326	55326	55326
28	92292	-60.64	57378	0.13	57454	57454	57454
29	92496	-55.24	59449	0.22	59582	59582	59582
30	92659	-50.15	61442	0.43	61710	61710	61710
31	92721	-45.24	64694	-1.34	63838	63838	63838

The second part of the convergence study is performed by simulating the response of the rod to an impulsive force applied to the left boundary for 1 second with a time step of $\Delta t = 10^{-6}$ s. The applied impulsive loading is presented in Figure 4.2. and is expressed mathematically as

$$F(t) = \begin{cases} P \sin^2\left(\frac{\pi}{\tau} t\right) & 0 \leq t \leq T \\ 0 & t > T \end{cases}, \tag{4.4}$$

where $\tau = 7.32 \times 10^{-5}$ s is the duration of the force and $P = 160000$ N is the amplitude of the applied force. The duration of the force is chosen based on the initial pulse observed in the experimental measurements in Chapter 3. Due to the linearity of the single rod system, only one applied force is considered in this work. The response is simulated using the *ode45* function in MATLAB® with relative and absolute tolerances of 10^{-8} and 10^{-9}, respectively. Due to the tolerances chosen and the fact that *ode45* uses a variable time step when integrating the response, no study is performed on the effect of the time step on the convergence of the model.

Since the boundary conditions are free-free, the rod possesses a rigid-body mode, which limits the use of the displacement response for determining the suitable number of elements. Instead, the velocities of the left and right boundaries are used to identify the optimal number of elements for modeling the rods. A comparison of the velocities for the 1-second simulation is presented in Figures. 4.3(a) and (b) for the left and right boundaries, respectively. The comparison shows that the velocities for all five models agree well in terms of the overall response; however, greater insight is gained by zooming into the response at the beginning of the response, around 0.1 s, and at the end of the response. The zoomed-in views at the beginning and around 0.1 seconds are shown

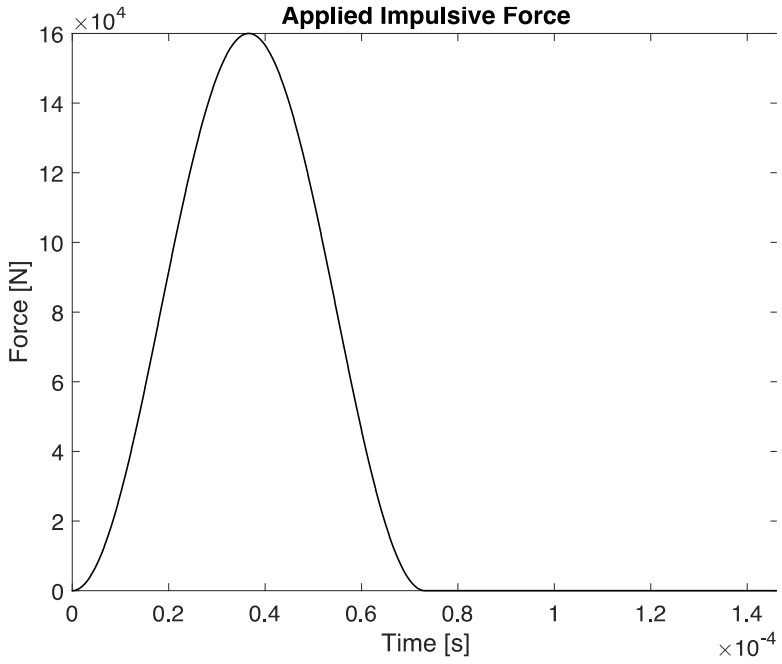

Figure 4.2 The impulsive force applied to the left boundary of the rod.

for the left boundary in Figures 4.4(a) and (b), respectively. These views show that in the beginning only the five- and ten-element models differ significantly from the other models with the 5-element model showing the greatest difference. The difference in the early-time response is attributed to the differences in the errors of the higher modes of the five- and ten-element models. By 0.1 seconds all of the models have converged to the same response with only a small difference observed in the 5-element model. At the end of the simulation (1 second), all of the response of all models are the same, indicating long-term convergence of the models as shown in Figures 4.5(a) and (b). Based on the results of this convergence study, the ten-element model was selected and all results following this section are created using this model. Lastly, the ten-element model is

compared with the FE model from Chapter 3 for 0.1 seconds in Figure 4.6., which shows good agreement between the two models.

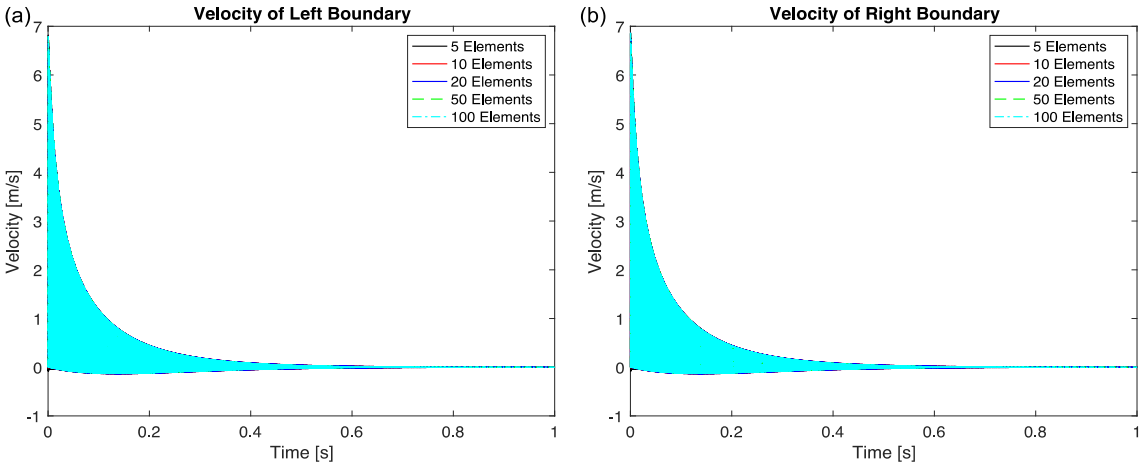

Figure 4.3 The comparison of the velocities of the (a) left boundary and (b) right boundary for the SE models consisting of 5, 10, 20, 50, and 100 elements.

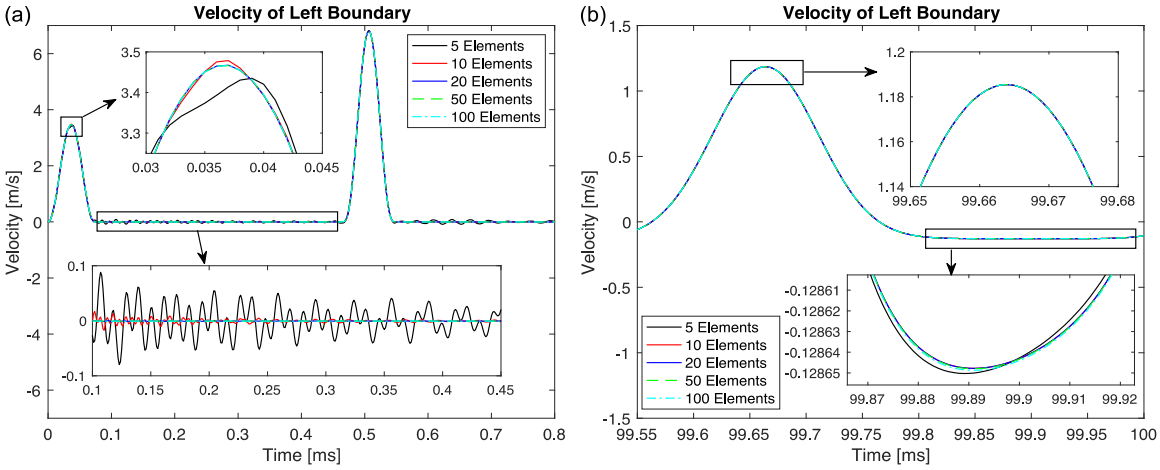

Figure 4.4 The comparison of the velocity of the left boundary at (a) the beginning of the simulation and (b) around 0.1 seconds for the SE models consisting of 5, 10, 20, 50, and 100 elements.

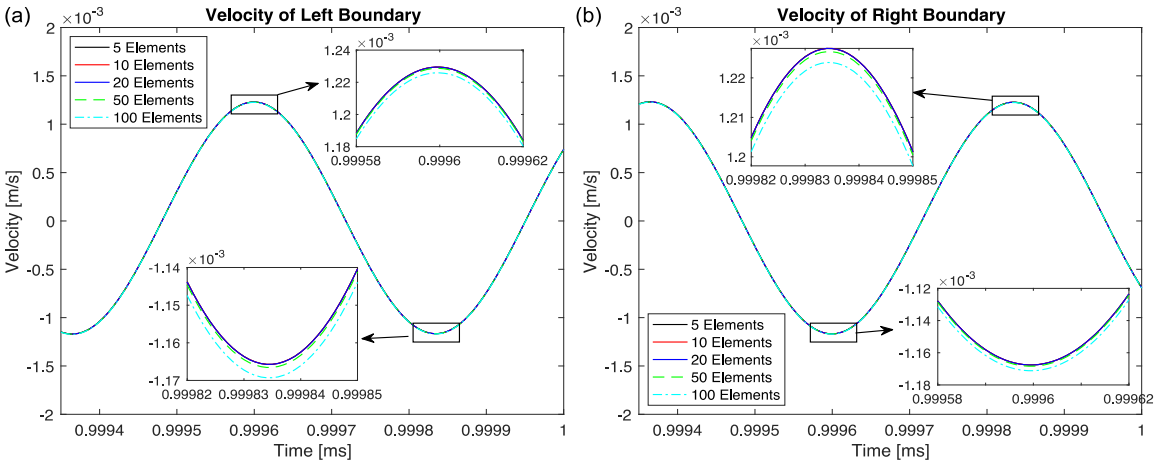

Figure 4.5 The comparison of the velocity at the end of the simulation for (a) the left boundary and (b) the right boundary for the SE models consisting of 5, 10, 20, 50, and 100 elements.

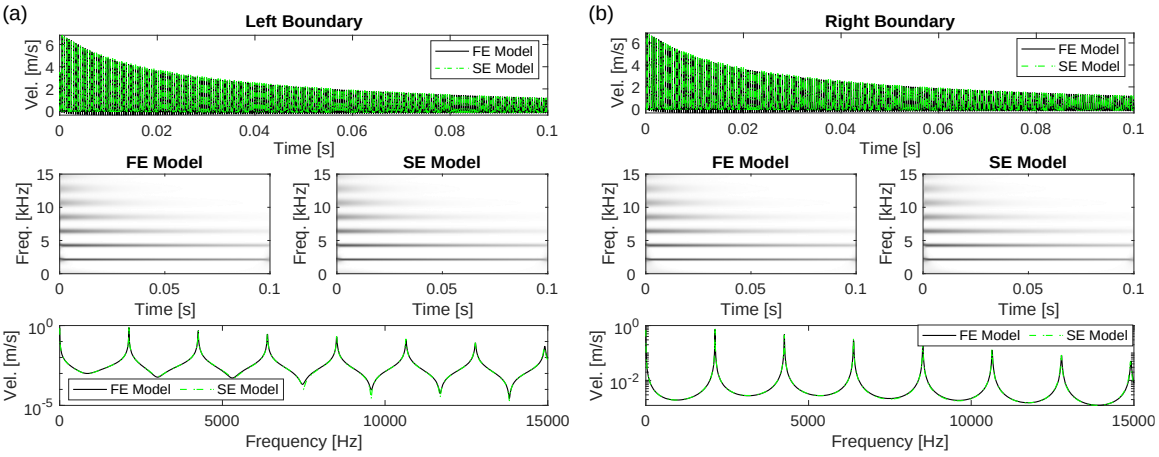

Figure 4.6 Comparison of the SE model with the FE model used in Section 3 for the applied force depicted in Figure 4.2. for (a) the velocity of the left boundary and (b) the velocity of the right boundary.

4.3. Natural Frequency and Mode Shape Transitions for Varying Torques

Since the stiffness of each joint depends on the corresponding torque, the resulting natural frequencies and mode shapes of the assembled system also depend on the torques.

Thus, the dynamics of the structure transitions from a fully coupled system to three uncoupled rods as the joints loosen. Although these transitions are nonlinear due to the model used for the instantaneous torque, at any instant in time the joint can be approximated by a linear spring and, thus, the system be modeled using linear modes of vibration. Thus, to explore these transitions prior to simulating the actual response of the structure, the natural frequencies and mode shapes are computed as the torque in each joint varies. Figure 4.7(a) presents the natural frequency transitions as the torque in each joint is varied equally and Fig. 4.7(b) presents the transitions for the case where the torque in the first joint is fixed at the theoretical maximum torque of 77.42 Nm and the torque in the second joint is varied. The natural frequency transitions reveal that the dynamics can be

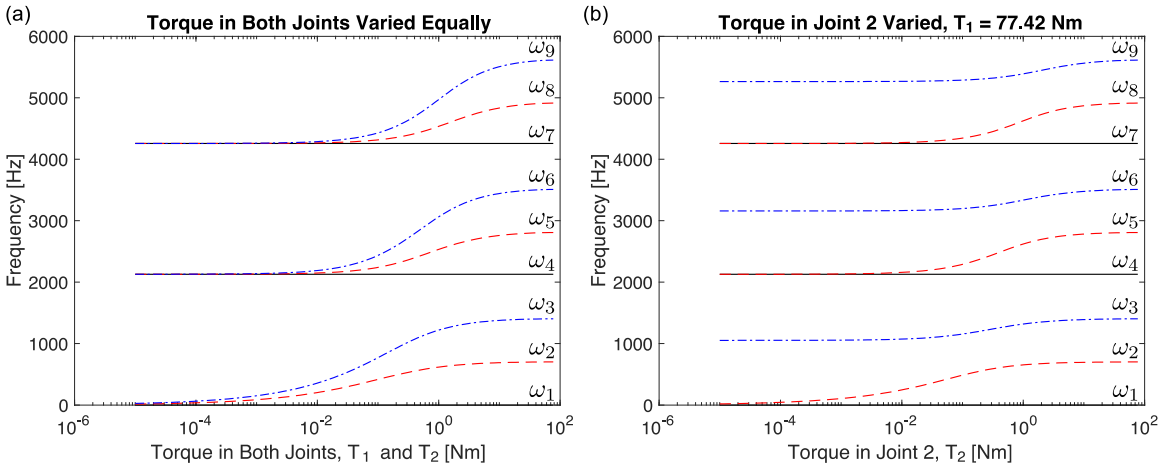

Figure 4.7 Transitions of the natural frequencies of the system as (a) the torque in both joints are varied equally and (b) the torque in the first joint is fixed at the theoretical maximum torque of 77.42 Nm and the torque in the second joint is varied.

divided into three different regimes: (1) a linear regime at low torque where the rods are effectively uncoupled, (2) a transition regime where the natural frequency depends

strongly on the torque inside each joint, and (3) a second linear regime at high torque where the rods are strongly coupled and act as a single rod of length $3L$. In the low-torque linear regime, the rods are effectively uncoupled and, thus, each natural frequencies is repeated three times such that $\omega_{3n+1} = \omega_{3n+2} = \omega_{3n+3}$ for $n = 0,1,2, \ldots$. As the joints are torqued, the natural frequencies ω_{3n+2} and ω_{3n+3} increase and transition away from ω_{3n+1}, which remains unaffected by the change in torque of the joints. Note that if only one of the joints is torqued, then only one of the three repeated natural frequencies transitions. Finally, in the high torque regime (both joints tightened), all of the natural frequencies are distinct and are comparable to the natural frequencies of a solid rod with length $3L$. Comparing the transitions depicted in Figure 4.7(a) with those in 4.7(b) reveals that the transitions depend on the torque in each joint, such that there are an infinite number of possible transitions and that the actual transition taken during dynamic loosening will depend on the initial torques of each joint.

Throughout all three regimes, the natural frequency of $3n + 1$ mode remains unchanged as the torques of the joints are increased. One might hypothesize that the reason the $3n + 1$ mode remains unchanged is because it exhibits a node at each interface and, thus, changes in the joints do not alter it. To investigate this hypothesis, the mode shape transitions are presented for second through fourth modes in Figures 4.8(a) and (b) for the case of equally varied torque in each joint and the case of fixed torque in the first joint and the torque in the second joint varied, respectively. The first mode is neglected because it is unaffected by the change in torques and is a rigid body mode with amplitude

of unity at all positions for all torques. The mode shapes reveal, in both cases, that the second and third modes begin as rigid body modes at low torques

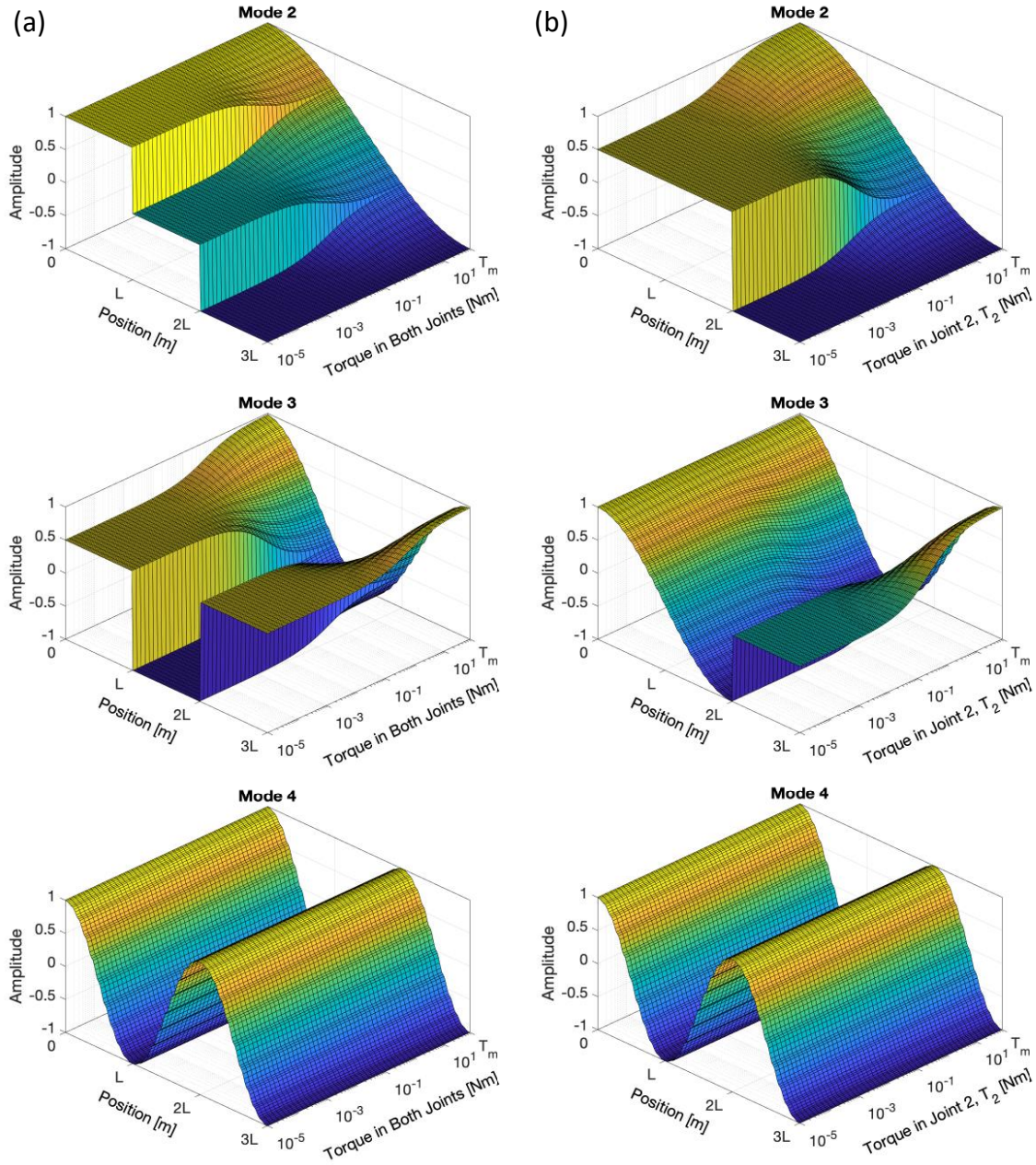

Figure 4.8 Transitions of the second, third, and fourth mode shapes as (a) the torques in both joints are varied equally and (b) the torque in the second joint is varied while the torque in the first joint remains fixed at the theoretical maximum torque of 77.42 Nm.

and transition into flexible modes as the torques of the joints is increased. The fourth mode corresponds to one of the repeated modes whose natural frequency is not affected by changes in the torques. As seen in Figure 4.8, the mode shape of the fourth mode is also unaffected by the changes in the torque, but, more importantly, it exhibits anti-nodes at the locations of each joint. A deeper investigation revealed that the fourth mode is only affected by torques that are less than 10^{-15} Nm; however, such a torque is not physically realistic and are an artifact of the assumptions made in the proposed modeling approach.

4.4. Investigation of the Behavior of the Theoretical System

To investigate how the two joints interact with each other through the global dynamics of the structure, the response to a square pulse is simulated for 0.5 seconds for three sets of initial torques: Case 1 – $T_1(0) = T_2(0) = 54$ Nm; Case 2 – $T_1(0) = 54$ Nm, $T_2 = 27$ Nm; and Case 3 – $T_1(0) = 27$ Nm, $T_2(0) = 54$ Nm. The applied square pulse has the form of

$$F(t) = \begin{cases} P & 0 \le t \le t_f \\ 0 & t > t_f \end{cases}, \tag{4.5}$$

where P is the amplitude of the pulse and t_f is the duration. In the initial set of simulations, we consider the behavior of the system for $P = 120$ kN and $t_f = 73.2\,\mu$s, which corresponds to the duration of the experiments discussed in Chapter 3 and an impact velocity of approximately 12 m/s.

We consider the strain at the center of each rod and plot the time series and corresponding wavelet spectra in Figure 4.9 for each set of initial conditions. Note that the left and right columns of Figure 4.9 depict the comparison of the strains in the first

and second rods and the first and third rods, respectively. Considering Case 1 (i.e., $T_1(0) = T_2(0) = 54$ Nm), we find that the strains in each rod are similar for first 0.06 seconds of the response. However, after 0.06 seconds all of the strains abruptly diverge from each other and settle into responses with different amplitude but similar frequency content. Specifically, the wavelet spectra for each rod reveal rich responses with many different harmonics participating before 0.06 seconds, but afterwards this rich behavior transitions into motion at only one or two frequencies. Furthermore, the fifth and sixth harmonics clearly decrease in frequency after 0.06 seconds and ultimately merge with the fourth harmonics, which mirrors the transitions of the linear natural frequencies discussed in the previous section. Thus, the transitions clearly result from the loosening of the joints, which will be investigated in detail after the next paragraph. Furthermore, these transitions could give rise to strongly nonlinear resonances in the dynamics, and this is further suggested by the beating pattern that can be observed between the strains of second and third rods around 0.07 seconds. This line of research is not investigated here and is left open for future work.

Considering the other two cases, the responses of all three rods are similar for the first 0.01 seconds, after which they abruptly change. However, unlike Case 1, the responses of only two of the rods are similar and are substantially different than the response of the remaining rod. Specifically, in Case 2, the responses of the first and second rods are comparable (nearly mirror images) after the transition whereas in Case 3 the strains of the second and third rods are similar. The fact that the strains of the first and

second rods are similar in Case 2 and the second and third rods in Case 3 correlates with the second and first joints having lower initial torques in each case, respectively. This

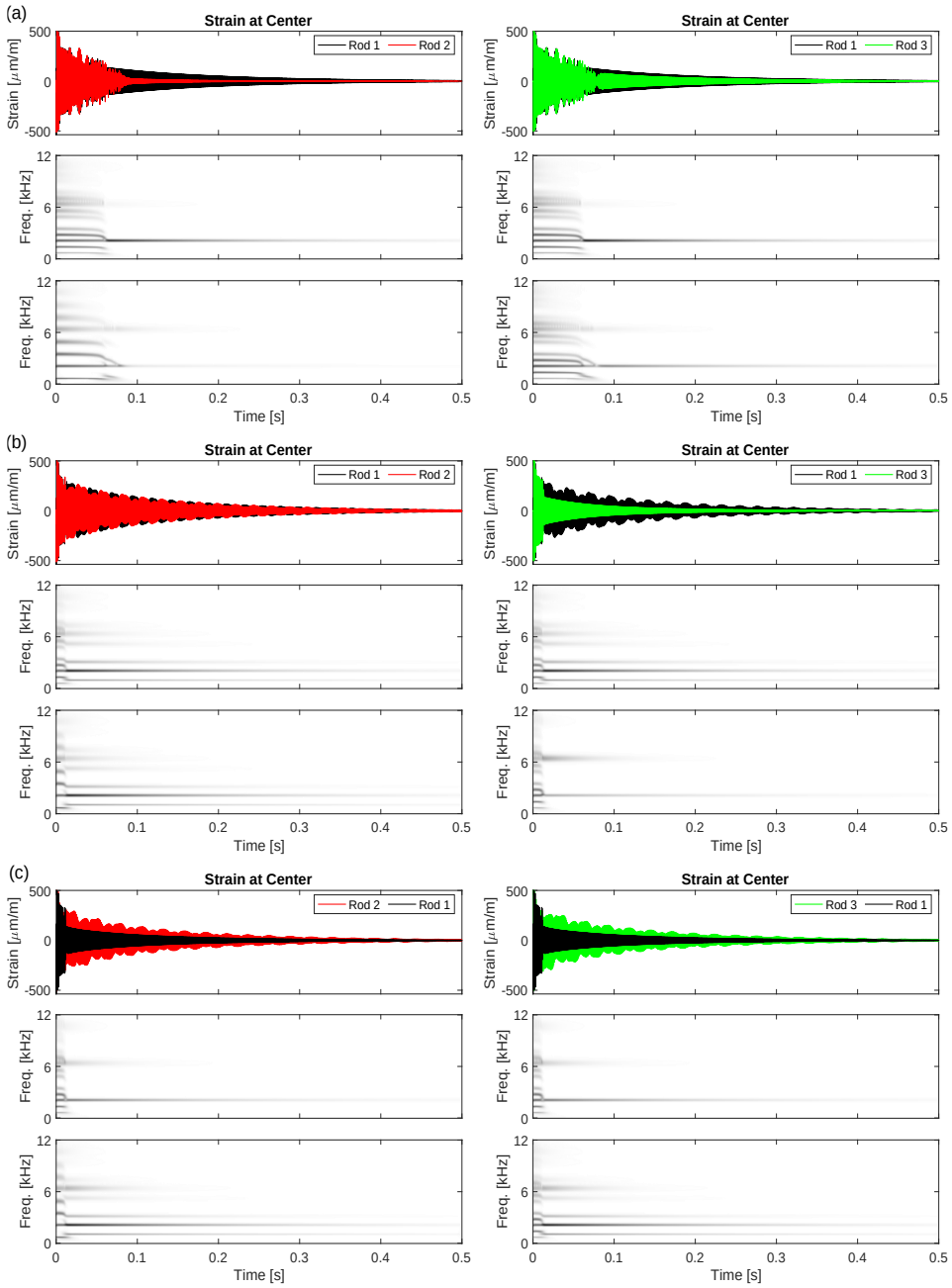

Figure 4. 9 Comparisons of the strain time series and corresponding wavelet spectra predicted at the centers of the rods for initial torques of (a) $T_1(0) = T_2(0) = 54$ Nm, (b) $T_1(0) = 54$ Nm, $T_2 = 27$ Nm, and (c) $T_1(0) = 27$ Nm, $T_2(0) = 54$ Nm.

indicates that, in Case 2, only the second joint loosens completely, such that the remaining torque in the first joint is high enough to couple the first and second rods together. Likewise, in Case 3, only the first joint loosens completely and the remaining torque in the second joint is large enough to couple the second and third rods together for the remainder of the response. We investigate these observations in detail in the next paragraph, but before doing so we now consider the frequency content as observed in the wavelet spectra. Similar to Case 1, the wavelet spectra of each rod reveal rich, multi-harmonic frequency content before the transition. However, unlike Case 1, only the third rod in Case 2 and the first rod in Case 3 transition into motion at only a relatively few frequencies. The first and second rods in Case 2 and the second and third rods in Case 3 transition to a multi-harmonic response at frequencies that correspond to the natural frequencies of a two-rod system coupled by a single joint like that studied in Chapter 3. These transitions provide further evidence that only the second and first joints loosen fully in Cases 2 and 3, respectively, unlike Case 1 where both joints loosen completely.

To substantiate the observations made previously, we depict the instantaneous torque in each joint for all three cases in Figure 4.10. Considering Case 1 first, the loss of torque in each joint is comparable with only a small deviation arising at as the torques approach zero. Considering Case 2, the two torques follow a similar trend initially, but diverge significantly after the second joint approaches zero. Specifically, the rate of loss of torque in the first joint abruptly changes as soon as the second joint loosens completely, which prevents the first joint from loosening fully. The remaining torque in the first joint at the end of the simulated response is 14.45 Nm, which corresponds to a

stiffness of 4.47×10^9 N/m. This confirms the observations made previously that only the second joint loosens completely in Case 2. Considering Case 3 now, the instantaneous torques in each joint again follow similar trends initially but diverge significantly after the first joint loosens completely. Specifically, similar to Case 2, the rate of loss of torque of the second joint abruptly changes after the first joint loosens completely, which corresponds to a change in the dynamics of the system and prevents the second joint from loosening fully. The remaining torque in the second joint at the end of the simulated response is 20.19 Nm and the corresponding stiffness is 5.28×10^9 N/m. This confirms the observations that only the first joint loosens entirely in Case 3. Interestingly, even though Case 3 is effectively the opposite of Case 2, the remaining torque in the second joint in Case 3 is higher than that in the first joint in the second case. This suggests that the remaining torque in each joint depends on the behavior and loosening of the other joint, which forms the basis of the investigation of the next section.

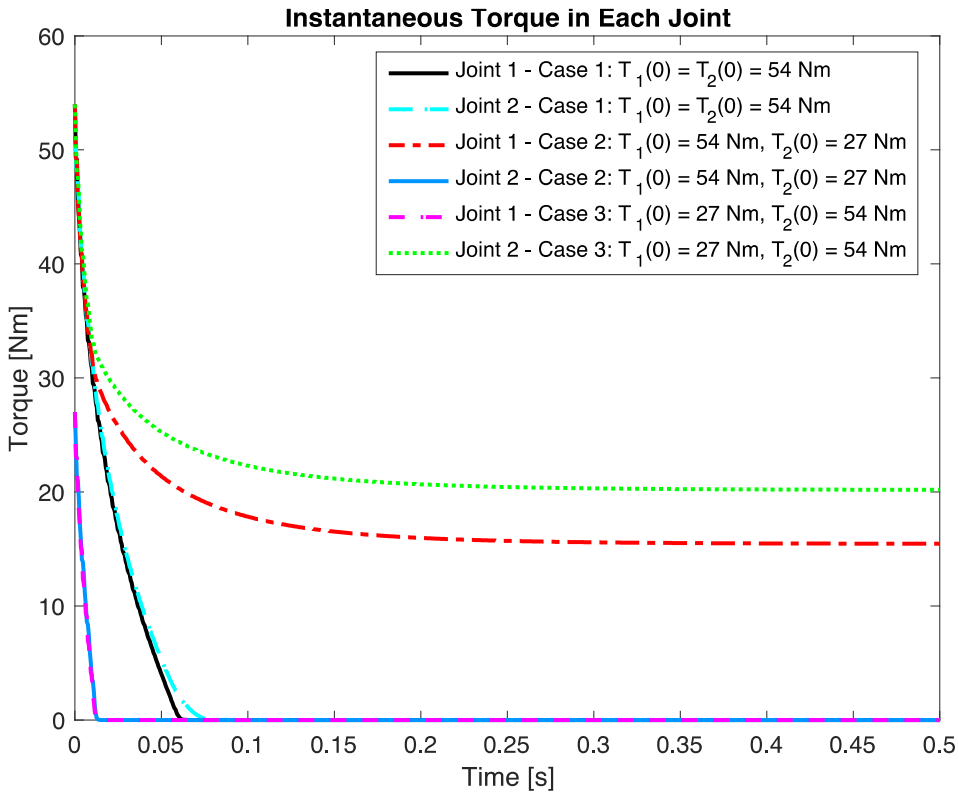

Figure 4.10 Comparisons of the instantaneous torque in each joint for the three different sets of initial conditions.

4.4. Overview of the Effect of the Loosening of One Joint on the Other

We investigate the effect of the initial torques of one joint on the loosening of the other joint by simulating the response of the system to the square pulse given in Eq. 4.5 for different forcing amplitudes and different combinations of initial torques. Specifically, we simulate the response for 1 second for 10,000 combinations of initial torques by considering 100 initial torques for each joint in the range of [14,54] Nm and for forcing amplitudes of $P \in [10,1000]$ kN. The forcing amplitude is considered in increments of 10 kN from 10 to 100 kN, increments of 5 kN from 100 to 200 kN, increments of 10 kN from 200 to 500 kN, and increments of 50 kN from 500 to 1000 kN. Based on the results of these simulations, we define the following five regimes of behavior: Regime I: Independence, $0 \leq P \leq 50$ kN; Regime II: Weak Dependence, $50 < P \leq 80$ kN; Regime III: Strong Dependence, $80 < P \leq 120$ kN; Regime IV: Bands of mitigation, $120 < P \leq 380$ kN; and Regime V: Complete Rapid Loosening of the First Joint, $P > 380$ kN. Note that forcing ranges reported for each regime represent the general range of forces as the transitions from one regime to another are smooth and do not correspond to a discrete forcing value. These results are discussed in detail for each regime separately in the coming subsections.

4.5. Regime I: Independence, $0 \leq P \leq 50$ kN

To investigate the first regime, we depict the remaining torque in each joint after 1 second of response in Figures 4.11(a) and (b) for forces of 20 kN and 50 kN, respectively. Considering both cases simultaneously, we find that the remaining torque in the first joint is characterized by vertical bands of constant torque, which indicates that

the loosening of the first joint is independent of the initial torque in the second joint. The remaining torque in the second is exhibits similar behavior with horizontal bands of constant torque indicating that the loosening of the second joint is independent of the initial torque in the first joint. Moreover, the remaining torque in one joint is the mirror image of the other joint, which implies that the evolution of each joint is unaffected by changes in the global dynamics of the structure resulting from the loss of stiffness. Note that in this work we have assumed that as the force decreases, the loss of torque in each joint also decreases and no dependence will arise between the joints at forces lower than 20 kN. However, if other regimes do exist, then these are likely to be overshadowed by a minimal loss of torque in each joint, such that the dependence may not be important from a design perspective for single shock loading events. Considering now Table 4.2 for the case where $T_1(0) = 41.88$ Nm and $T_2(0)$ is varied, we find that the remaining torques in the first joint, $T_1(1)$, is equal to 40.18 for all three initial torques chosen for the second joint. Likewise, considering Table 4.2 for the case where $T_2(0) = 41.88$ Nm and $T_1(0)$ is varied, the remaining torques in the second joint, $T_2(1)$, are all close to 40.20 Nm. Thus, the remaining torques in each case confirm that the two joints behave independently of each other in this regime.

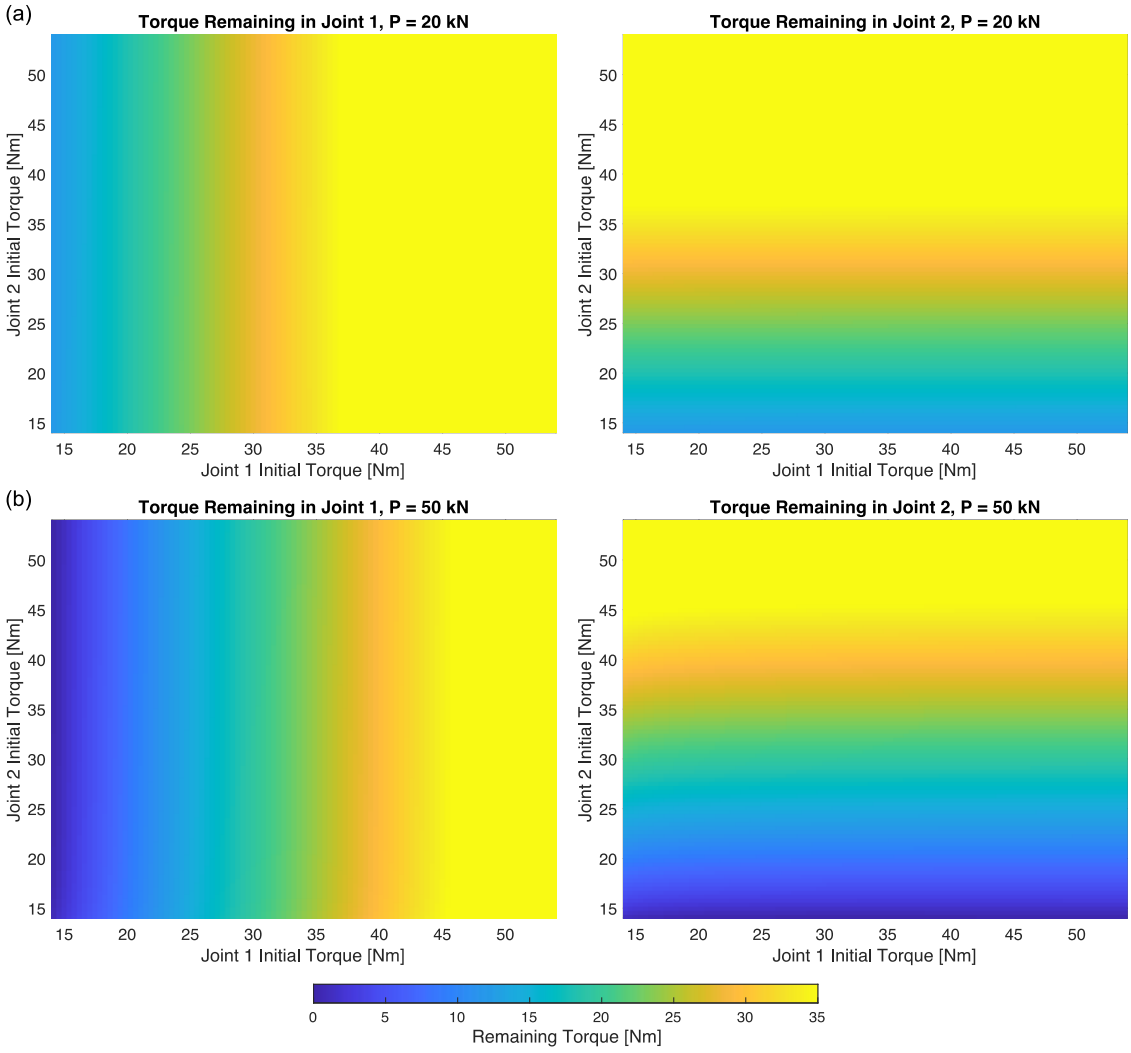

Figure 4.11 The remaining torques in each joint for excitation forces of (a) 20 kN and (b) 50 kN, corresponding to inside and the upper limit of Regime I: Independence, respectively.

Table 4.2 The remaining torques in each joint for cases where the initial torque in one joint is fixed and the other varies for Regime I.

Case	$T_1(0)$ [Nm]	$T_2(0)$ [Nm]	$T_1(1)$ [Nm]	$T_2(1)$ [Nm]
Torque in Joint 1 Fixed	41.88	49.96	40.18	48.22
	41.88	35.82	40.18	34.17
	41.88	21.68	40.18	19.97
Torque in Joint 2 Fixed	49.96	41.88	48.19	40.20
	35.82	41.88	34.15	40.21
	21.68	41.88	19.97	40.24

4.6. Regime II: Weak Dependence, $50 < P \leq 80$ kN

To investigate the second regime, we depict the remaining torque in each joint for excitation forces of 55 kN and 80 kN in Figures 4.12(a) and (b), respectively. Considering the case of 55 kN first, which is near the lower limit of this regime, we find that the remaining torque in the first and second joints are primarily characterized by vertical and horizontal bands just as in the previous regime, which indicates independence. However, when both joints have initial torques below 20 Nm, corresponding to the bottom left corner of each plot, the remaining torque of one joint shows weak dependence on the initial torque of the other one. As mention previously, the transitions between each regime are smooth and cannot be attributed to a discrete value of excitation force, such that the case of 55 kN could be considered either weak dependence or independent. However, from a design perspective, the 55 kN case could be treated as independent without much consequence for single shock loading conditions.

Considering now the case of 80 kN, we find that when the initial torque of one joint is less than or equal to 31 Nm, its remaining torque is dependent on the initial torque in the other joint. When the initial torques of both joints are above 31 Nm, then the remaining torque of one joint is weakly dependent on the other one. Thus, this regime can be separated into initial conditions where the evolution of the joints depend on each other and initial conditions where their evolutions are independent of each other. To illustrate this point further, consider the cases presented in Table 4.3 where $T_1(0) = 41.88$ Nm and three different initial torques in the second joint: $T_2(0) = 49.96$ Nm, $T_2(0) = 35.82$ Nm, and $T_2(0) = 21.67$ Nm. These initial conditions result in the following remaining torques

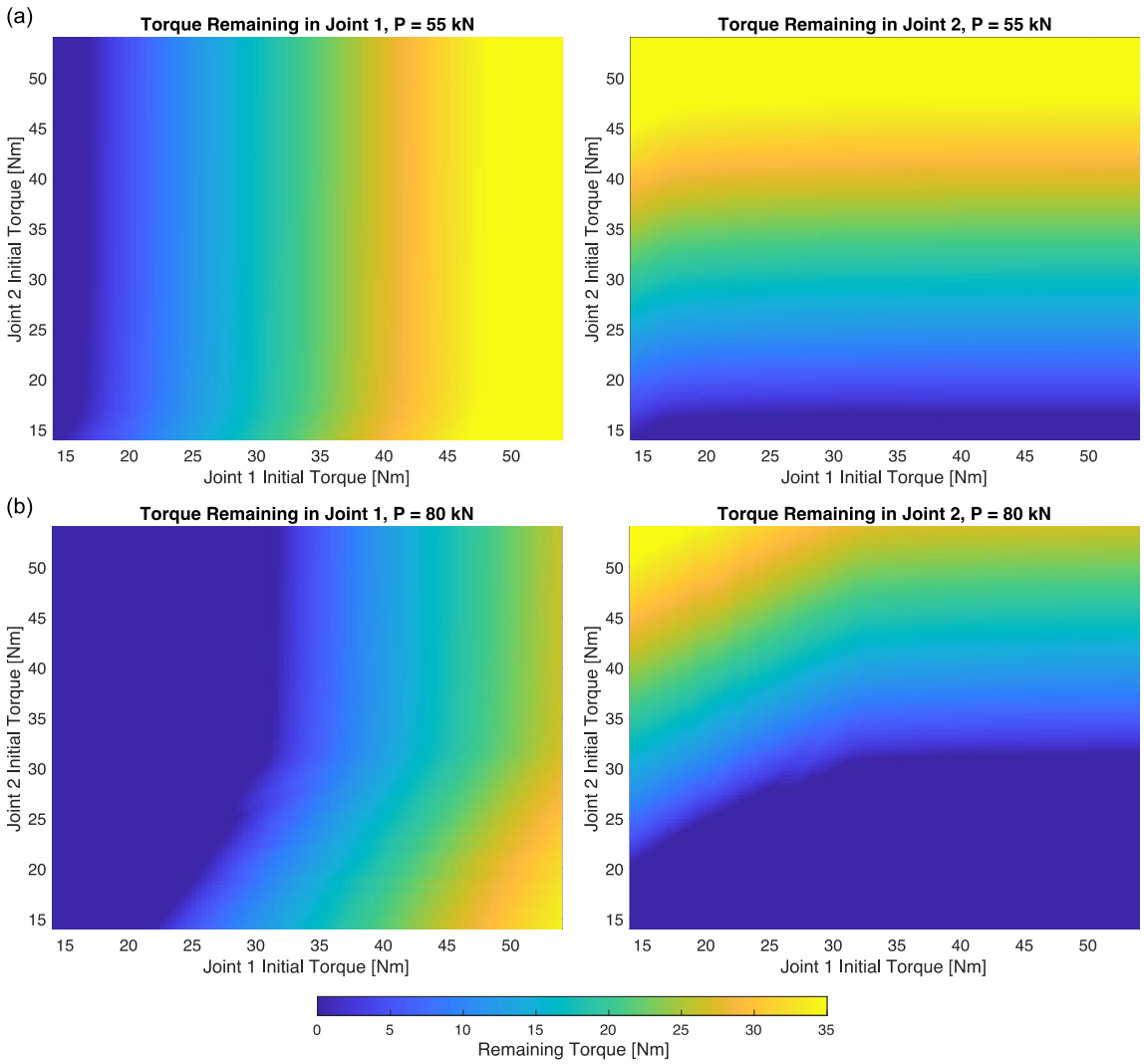

Figure 4.12 The remaining torques in each joint for excitation forces of (a) 55 kN and (b) 80 kN, near the lower limit and at the upper limit of Regime II: Weak Dependence, respectively.

in the first joint: $T_1(1) = 14.86$; $T_1(1) = 15.17$ Nm; and $T_1(0) = 20.39$ Nm. For the two cases where $T_2(0) > 31$ Nm, the remaining torques in the first joint are comparable indicating a weak dependence on the initial torque in the second joint. However, for the case where $T_2(0) < 31$ Nm, the remaining torque in the first joint is about 33% larger

than the other two cases even though the initial torque is the same in all three cases. Considering the data in Table 4.3where $T_2(0)$ is fixed at 41.88 Nm and $T_1(0)$ is varied at the same values as $T_2(0)$ in the previous case, we find that the remaining torques in the second joint are 15.17, 15.65, and 22.06 Nm, which illustrates a similar behavior as that observed for the first joint in Table 4.3. Thus, this analysis demonstrates that the evolution of one joint depends on the initial torque in the other joint.

Table 4.3 The remaining torques in each joint for cases where the initial torque in one joint is fixed and the other varies for Regime II.

Case	$T_1(0)$ [Nm]	$T_2(0)$ [Nm]	$T_1(1)$ [Nm]	$T_2(1)$ [Nm]
Torque in Joint 1 Fixed	41.88	49.96	14.86	23.53
	41.88	35.82	15.17	8.321
	41.88	21.67	20.39	0
Torque in Joint 2 Fixed	49.96	41.88	23.10	15.17
	35.82	41.88	7.967	15.65
	21.68	41.88	0	22.06

4.7. Regime III: Strong Dependence, $80 < P \leq 120$ kN

We investigate the third regime by depicting the remaining torque for forces of 80 kN and 120 kN in Figure 4.13(a) and (b), respectively. Considering first the case of 90 kN, we find that the remaining torques are comparable to those from the 80 kN case, except that now the joints exhibit only weak dependence when they start with an initial torque of 40 Nm or greater. Thus, the joints are dependent on each other for the majority of the initial torques selected in this study (which correspond to the range of torques investigated in previous experiments as discussed in Chapter 3). Interestingly, the maximum remaining torque in either joint occurs when that joint starts with an initial

torque of 54 Nm and the other one starts with an initial torque of 14 Nm. Moreover, when both joints begin with initial torques of 54 Nm, they both loosen to around 19 Nm of torque (specifically, $T_1(1) = 19.10$ Nm and $T_2(1) = 19.56$ Nm). Thus, when the initial torques in both joints are relatively large, the system will not completely loosen and remains coupled although at lower stiffnesses. These results suggests that the complete loosening of one joint may be prevented by manipulating the initial torque of the other joint, and we will explore this idea further in the next regime.

Considering the case of 120 kN shown in Fig. 4.13(b), we find that the remaining torques differ significantly compared to the case of 80 kN. One of the biggest differences is that there is no longer a set of initial torques where the joints exhibit only weak dependence, such that each joint depends on the other regardless of its own initial torque. Furthermore, the maximum remaining torque in either joint no longer occurs when the other joint begins with a torque of 54 Nm. Instead, the maximum remaining torque in the first and second joints occur when the second and first joints begin with torques of 16.02 Nm and 15.21 Nm, respectively. Moreover, the maximum remaining torque in the first joint is only 23.35 Nm whereas it is 30.52 Nm for the second joint, indicating that the evolutions of the joints are different unlike the previous regimes. Furthermore, bands where each joint does not loosen appear to be forming and this observation will be further developed in the next section. One of most interesting features is that whenever the joints have comparable initial torques (the diagonal band from the bottom left to top right), they both loosen completely regardless of the actual numerical values of the initial torques. This result contradicts the common idea that all the joints must be tightened to the same

level of preload to prevent them all from loosening and provides further support for the idea of manipulating the initial torque of one joint to control the loosening of the other joint.

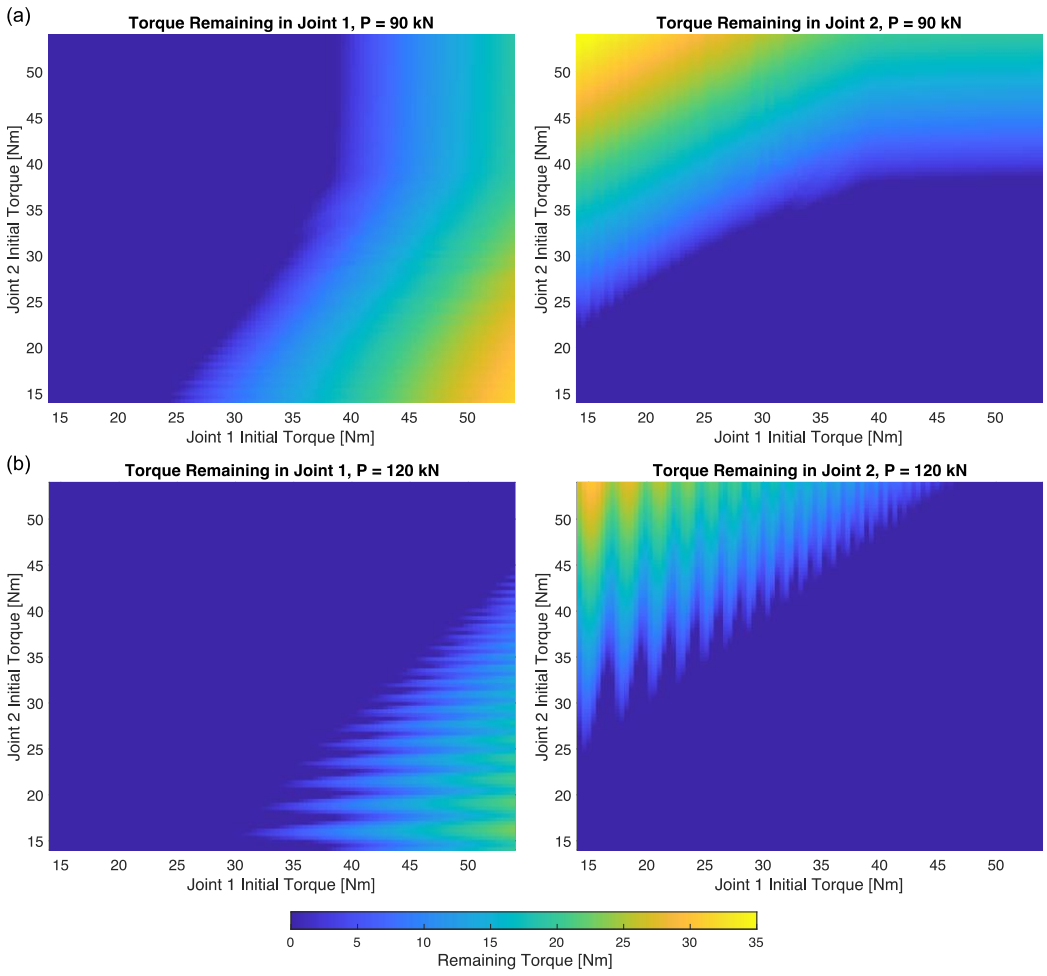

Figure 4.13 The remaining torques in each joint for excitation forces of (a) 90 kN and (b) 120 kN, near the lower limit and at the upper limit of Regime III: Strong Dependence, respectively.

4.8. Regime IV: Bands of Mitigation, $120 < P \leq 380$ kN

4.8.1. High-level Analysis of Regime IV

We explore the fourth regime by depicting the remaining torque in each joint for forces of 130 kN and 140 kN in Figure 4.14(a) and (b), respectively, and for forces of 160 kN and 350 kN in Figure 4.15(a) and (b), respectively. All four cases result in distinct bands in the remaining torque where the one of the joints does not loosen completely. In all cases, the bands for the first joint only occur when it starts with a relatively higher preload than the second joint and, similarly, the bands for the second joint only occur when its initial torque is much higher than that of the first joint. Furthermore, in all cases, there is a diagonal band of complete loosening in both joints corresponding to the cases where the joints begin with comparable torques. This result is the same as the observation made for the 120 kN case in the previous subsection and indicates a contradiction with the common idea that all joints should be preloaded to the same amount to prevent loosening. Note that there may be bands that appear below initial torques of 14 Nm (the lowest initial torque considered here); however, those torques are below what can be achieved by just tightening the joint by hand alone and are not investigated in this research. Moreover, a band of mitigation should always appear in the second joint if the first joint starts with a torque of zero or close to zero; however, this is a trivial case as the second and third rods are uncoupled to the first rod and, thus, the second joint will not be excited by the applied pulse. We divide the bands into strong and weak bands of mitigation, where a strong band is defined as being relatively long and maintains a torque greater than hand-tight (14 Nm) in the innermost region of the band. Conversely, a weak

band of mitigation corresponds to a band that is relatively short and has a remaining torque lower than hand-tight in its innermost region. Overall, there are six primary observations that can be made for this regime:

1) The number of bands of mitigation for each joint decreases as the applied force increases.
2) The torques for which the bands of mitigation occur change as the applied force changes.
3) The bands of mitigation for the first joint are distinct from those for the second joint in that they occur at different torques and have different lengths and bandwidths.
4) The bands of mitigation for the second joint are stronger than those of the first joint.
5) The widths of the bandgaps where both joints loosen completely increase as the applied force increases.
6) Whenever both joints begin with similar torques, they both loosen completely regardless of the actual numerical value of the initial torques.

We explore these observations in greater detail by examining each case individually and comparing the bands across different cases.

Considering the case of 130 kN, although the bands are distinct at lower torques, they are not fully developed at higher torques, which is indicated by the blending of the bands at higher torques. Interestingly, the bands for the second joint show an overall higher remaining torque than the bands for the first joint, which is most likely because the applied pulse reaches the first joint at nearly the maximum amplitude

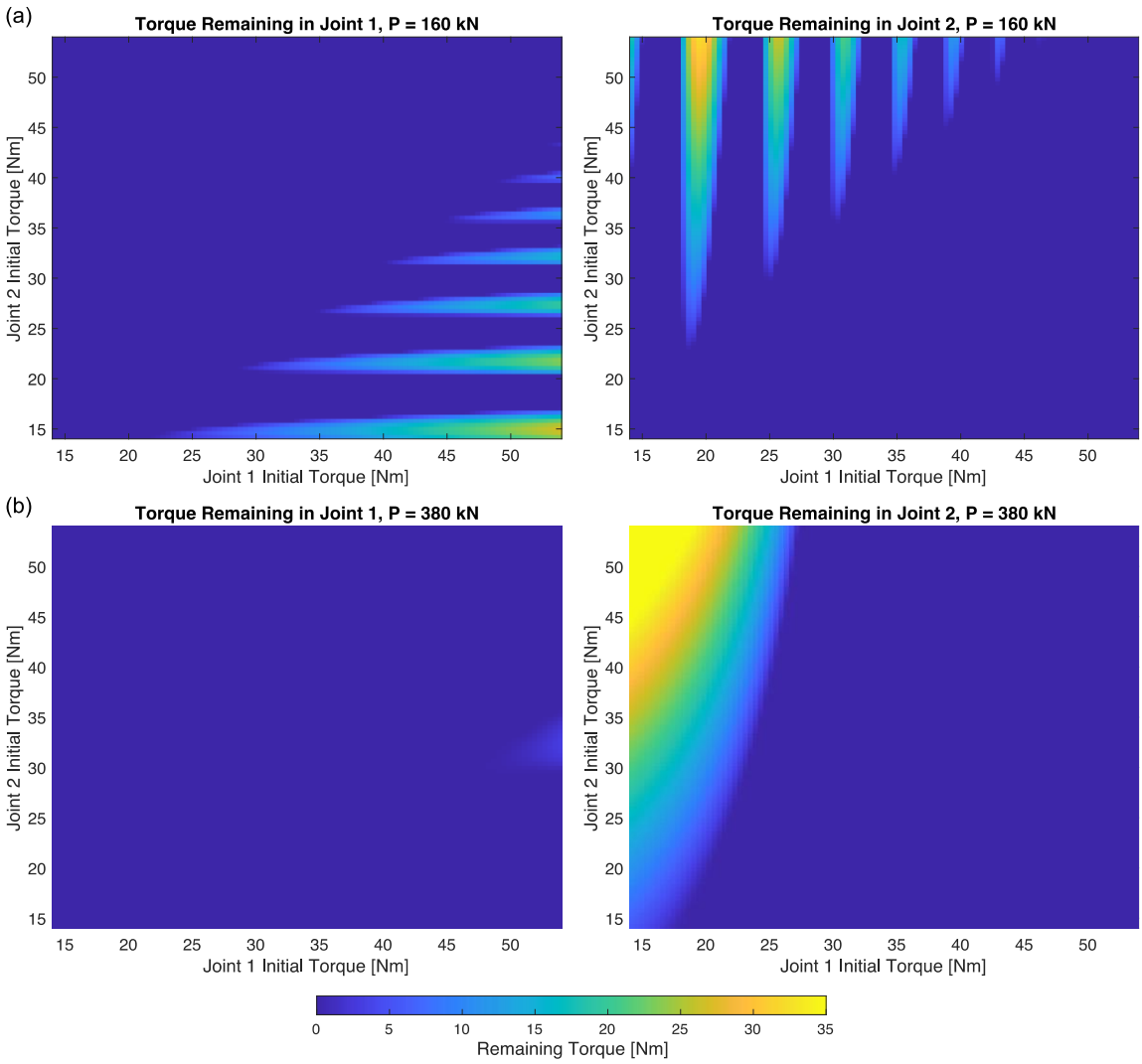

Figure 4.14 The remaining torques in each joint for excitation forces of (a) 160 kN and (b) 380 kN, inside and near the upper limit of Regime IV: Bands of Mitigation, respectively.

whereas the transmitted pulse that reaches the second joint is weakened due to reflections at the first joint. This idea is further supported by a comparison of the maximum remaining torque in each joint, which is 22.98 Nm for the first joint and 28.92 Nm for the second. The maximum remaining torque in the first joint occurs at $T_1(0) = 54$ Nm and $T_2(0) = 14.4$ Nm and the maximum for the second joint occurs at $T_1(0) = 17.23$ Nm

and $T_2(0) = 54$ Nm. Moreover, the total number of bands for the second joint is higher than that of the first joint. Specifically, the first joint exhibits 13 bands and the second joint contains 14 bands of mitigation. Of these, the first six bands of the first joint, counted from the bottom up, are strong bands of mitigation whereas the first eight bands of the second joint, counted from left to right, are strong.

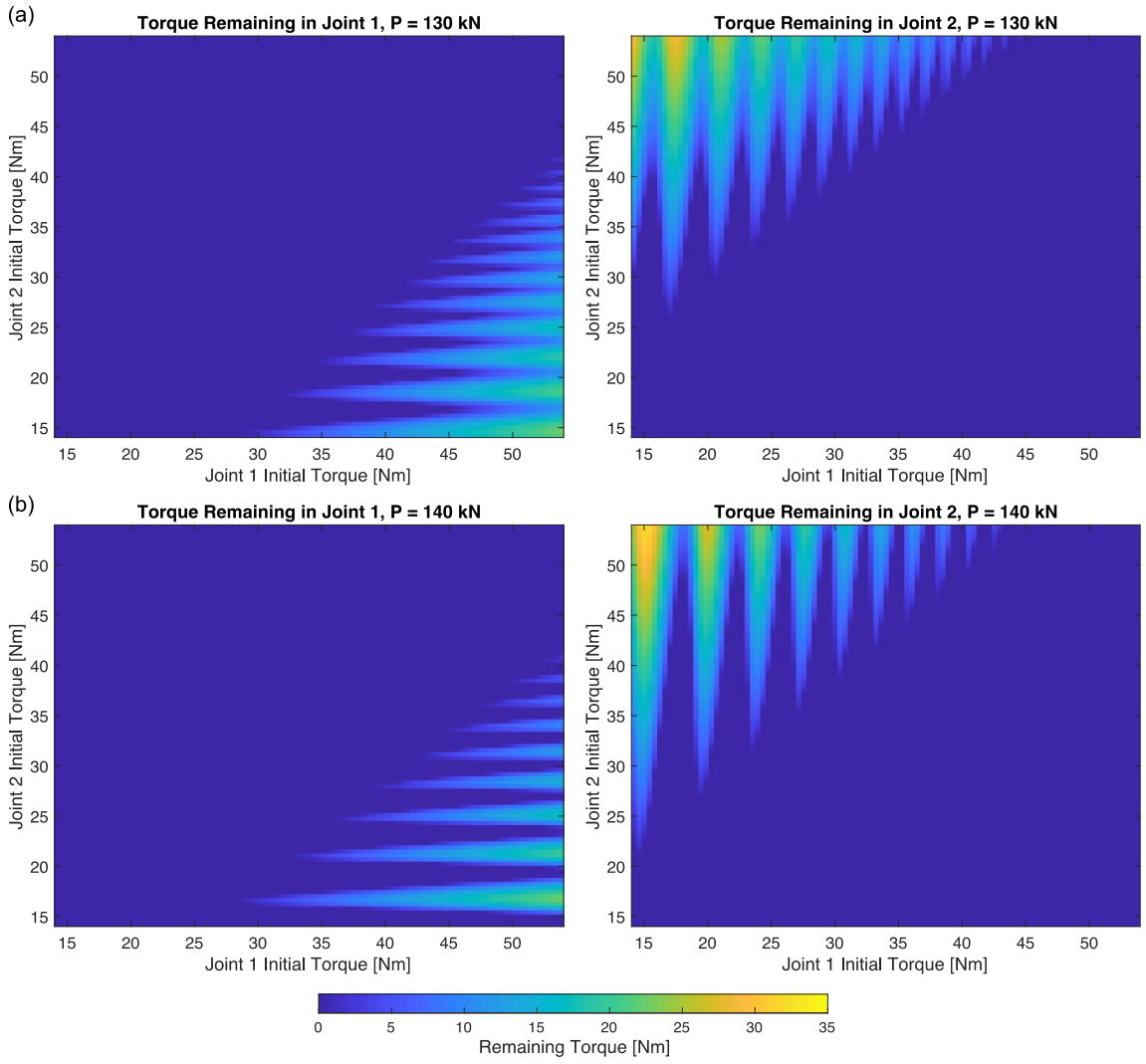

Figure 4.15 The remaining torques in each joint for excitation forces of (a) 130 kN and (b) 140 kN, near the lower limit and inside of Regime IV: Bands of Mitigation, respectively.

Considering now the case of 140 kN, it is seen that the bands are much more distinct compared to the 130 kN case with narrow gaps of complete losing arising between each band. Similar to the previous case, the bands for the second joint have a higher remaining torque than the bands observed for the first joint. The maximum remaining torque in the first joint is 22.8 Nm, slightly lower than in the previous case, which occurs for initial torques of $T_1(0) = 54$ Nm and $T_2(0) = 16.42$ Nm, with the latter initial condition being higher than in the case of 130 kN force. The maximum remaining torque in the second joint is 32.35 Nm, higher than in the previous case, and occurs for initial conditions of $T_1(0) = 15.21$ Nm and $T_2(0) = 54$ Nm, with the former initial condition being lower than in the previous case. Given that the initial conditions give rise to the maximum remaining torque for this forcing amplitude compared to previous forcing verified the second observation. Compared to the previous case, there are only 9 and 10 distinct bands for the first and second joints, respectively, which supports the first observation discussed earlier.

Now consider the case of 160 kN, depicted in Figure 4.15(a), which reveals that there are 6 and 7 distinct bands for the first and second joint, respectively, which validates the first observation stated previously. Compared to the case of 140 kN, the gaps between the bands are now much wider and both joints always completely loosen within the bandgaps, which verifies the fifth observation stated earlier. The maximum remaining torque of the first joint is 27.02 Nm and occurs at initial torques of $T_1(0) = 54$ Nm and $T_2(0) = 14.81$ Nm. The maximum remaining torque for the second joint is 32.48 Nm and occurs for initial torques of $T_1(0) = 19.25$ Nm and $T_2(0) = 54$ Nm. The

investigation into the underlying mechanisms that give rise to the bands of mitigation is left for the next section after the discussion of the final regime in the next subsection.

Finally, we consider the case of 380 kN depicted in Figure 4.15(b) where the remaining torques of both joints each show only a single band of mitigation unlike the previous cases. Note that the band of mitigation for the first joint is quite weak and corresponds to initial conditions of $T_1(0) \in [49.96, 54]$ Nm and $T_2(0) \in [29.76, 35.41]$ Nm. Within this band, the maximum remaining torque in the first joint is 3.334 Nm and corresponds to initial conditions of $T_1(0) = 54$ Nm and $T_2(0) = 32.18$ Nm. In contrast a single large band of mitigation appears for the second joints and corresponds to initial conditions of $T_1(0) \in [14, 26.93]$ Nm and $T_2(0) \in [14, 54]$ Nm. The maximum remaining torque for the second joint is 43.87 Nm and occurs for initial conditions of $T_1(0) = 14$ Nm and $T_2(0) = 54$ Nm. The fact that the maximum remaining torques in the first and second joints are so small and so large, respectively, implies that the force is so strong that it overwhelms the first joint and causes it to loosen completely within the first few passes of the stress wave. To verify this observation, we present the instantaneous torques for each joint for initial torques of 14, 54, and 54 Nm for the first joint and 54, 54, and 14 Nm for the second joint in Figure 4.16. The instantaneous torques reveal that when the first joint loosens completely within the first few passes of the stress wave regardless of its starting torque, which confirms the observations made earlier.

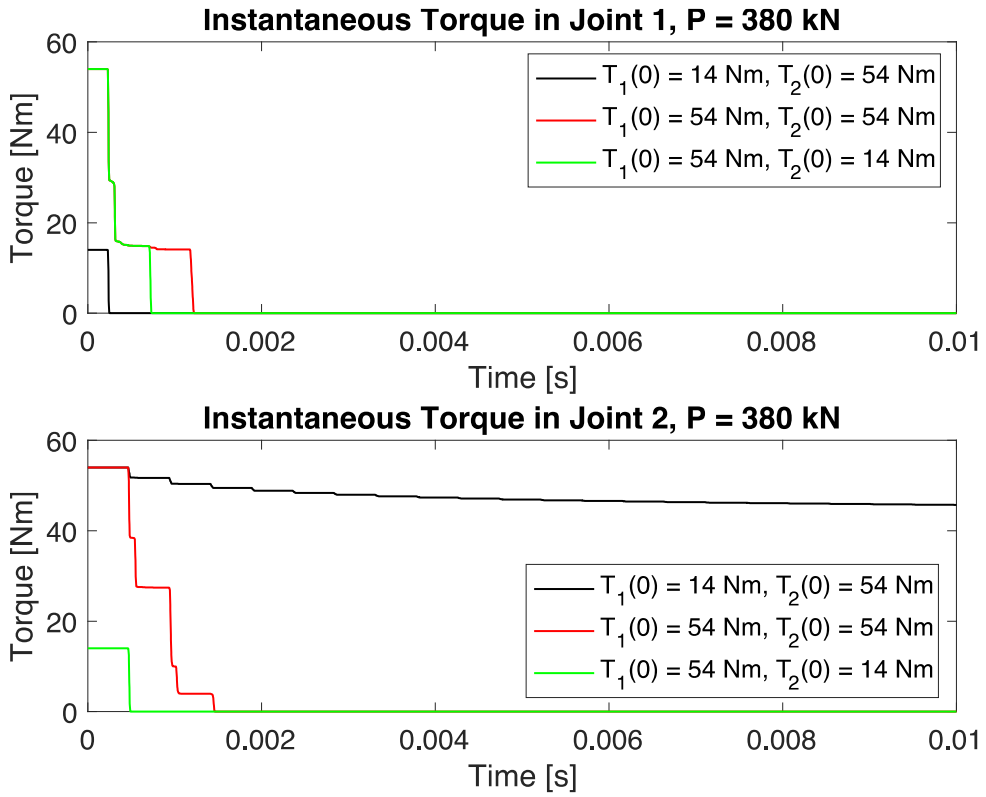

Figure 4.16 The instantaneous torques of each joint for a forcing amplitude of 380 kN for initial torques of 14, 54, and 54 Nm for the first joint and 54, 54, and 14 Nm for the second joint.

4.8.2. Investigation of into the Underlying Reasons for the Bands of Mitigation

To determine the reason for the bands of mitigation in Regime IV, we consider the remaining torques for an applied force of 160 kN and investigate the behavior of the system for twelve different initial conditions (a-l) as depicted on Figure 4.16. These cases correspond to combinations of initial torques of 17.64, 19.66, and 22.08 Nm for the first joint and 54, 43.49, 30.97, and 20.06 for the second joint. The initial and final torques for the twelve cases are provided in Table 4.4. Note that the numerical solution of the

differential equations governing the torque in each joint asymptotically approach zero and be less than the machine epsilon value; however, we report values below machine epsilon as zero and give the actual values above in Table 4.4.

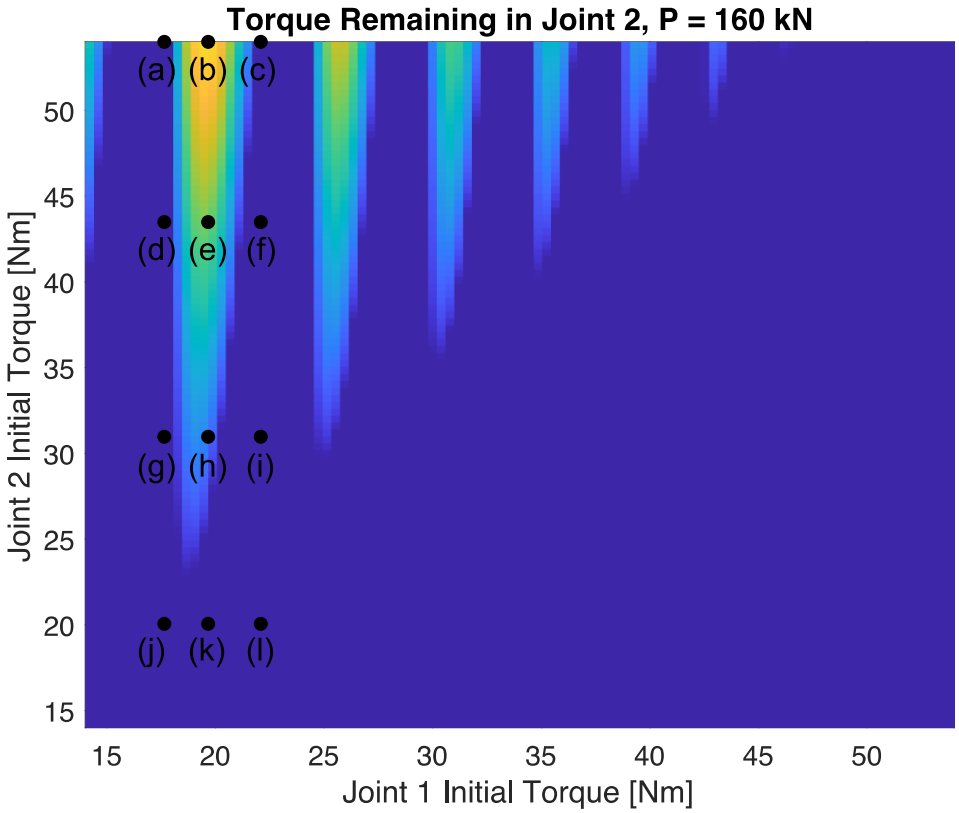

Figure 4.17 The remaining torque in the second joint for a force of 160 kN and the twelve cases selected to investigate the mechanisms governing the formation of the band of mitigation.

The instantaneous torques for each joint are depicted in Figure 4.18(a) for the entire simulation time of 1 second and 4.18(b) for the first 0.01 seconds. Considering first 4.18(a), little insight is gained from the instantaneous torque in the first joint because it loosens too quickly; however, the instantaneous torques of second joint reveal that each case results in a different rate of loosening and that the second joint stops loosening in

Table 4.4 The initial and final torques for each joint for the twelve cases a-l.

Case	First Joint [Nm]		Second Joint [Nm]	
	$T_1(0)$	$T_1(1)$	$T_2(0)$	$T_2(1)$
a	17.64	0	54	3.68×10^{-5}
b	19.66	0	54	31.77
c	22.08	0	54	8.25×10^{-11}
d	17.64	0	43.49	1.80×10^{-12}
e	19.66	0	43.49	21.82
f	22.08	0	43.49	0
g	17.64	0	30.97	6.55×10^{-13}
h	19.66	0	30.97	6.539
i	22.08	0	30.97	0
j	17.64	0	20.06	6.612×10^{-7}
k	19.66	0	20.06	0
l	22.08	0	20.06	0

cases b, e, and h after 0.25 seconds and well before the total simulation time. Considering now the zoomed-in views of the instantaneous torques in Figure 4.18(b), the instantaneous torques for the first joint show that all cases with the same initial torques the loss of torque is the same for the first 0.001 seconds where the loss of torque differs as the wave passes. However, despite the fact the actual losses of torque differ in each case, all of the cases except for case l loosen completely by 0.004 seconds. Case l loosens completely by 0.008 seconds. Considering the instantaneous torques of the second joint, we find that all of the cases that start with the same initial torque decay at the similar rates until around 0.0025 seconds at which point the torques diverge from each other. Specifically, cases b, e, h, and j all suddenly diverge from their original trajectories and begin loosening at comparable rates that are all significantly different than the other

cases. Of these four, case j is the only one not on the band of mitigation observed in Figure 4.17 and also corresponds to a different initial torque in the first joint ($T_1(0) =$ 17.64 Nm for case j), which reflects that there is some curvature observed for the band in Figure 4.17. Interestingly, the second joint loosens before the first joint in case l, which causes the decay in the first joint to abruptly change compared to the others. The reason for this is that the first joint begins with a higher torque than the second joint in case l, so it is more akin to cases where the first joint does not loosen but the second one does.

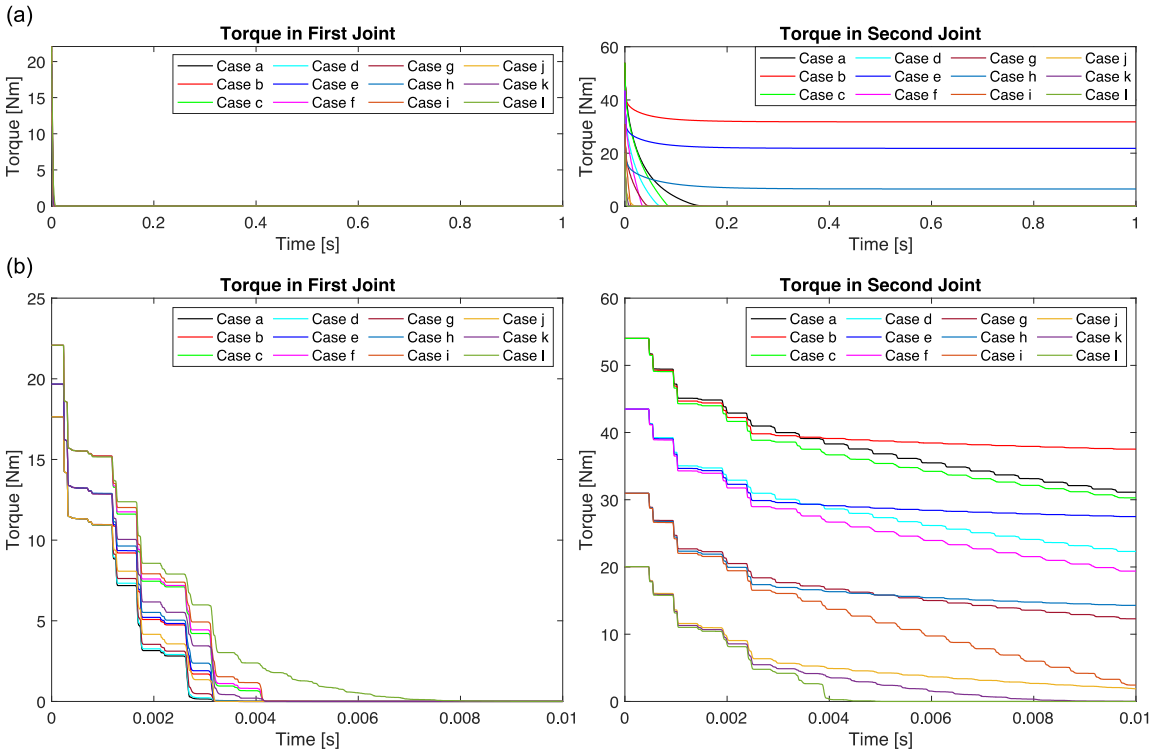

Figure 4.18 The instantaneous torques for each joint for cases a-l for (a) the entire simulation time of 1 second and (b) the first 0.01 seconds.

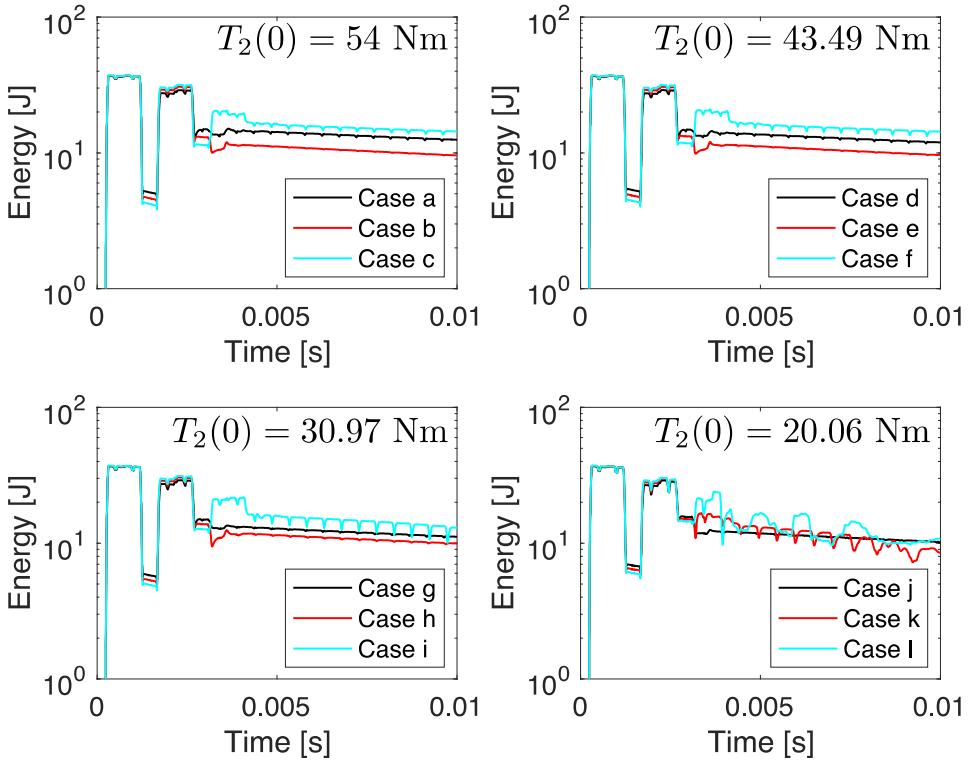

Figure 4.19 The sum of the instantaneous mechanical energy in the second and third rods neglecting any energy stored in the second joint. The perturbations or drops in the energies that look like spikes correspond to the neglected energy stored in the second joint.

To understand why the rates of loss of torque abruptly change for cases b, e, h, and j, we consider the summation of the total mechanical energy in the second and third rods and depict these in Fig. 4.19 for the four different initial torques in the second joint. The reason for summing the energy in the second and third rods is that when the first joint loosens completely, the result is that the system partitions itself into two separate systems of the first rod by itself and the second and third rods together. Prior to the first joint loosening, the total mechanical energy in the system is exchanged between all three rods; however, as soon as the first joint loosens, the energy is suddenly partitioned into a

portion that remains in the first rod for all time and a portion that gets exchanged between the second and third rods. Thus, by summing the total mechanical energy in the second and third rods, we can gain insight into how much energy is being exchanged between the rods and how this affects the loosening of the second joint. Note that, due to the way the coupling between the rods is implemented, the loosening of a joint results in a hysteresis effect and dissipates energy. As such, it is not clear how to calculate the potential energy that is stored inside the joint during the motion or how to separate it from the energy dissipated due to the hysteresis effects. However, whenever the relative displacement between the two rods is zero, then the total mechanical energy resides entirely in the two rods and can be determined by summing up the energy in each rod. To this end, we neglect any energy stored in the second joint and consider only the summation of the mechanical energy in the second and third rods and recognize that any oscillations or sudden drops in the resulting curves correspond to the missing energy stored in the joint.

As can be seen in Figure 4.19, the instantaneous mechanical energies of all cases follow similar trends for approximately the first 0.025 seconds after which the cases diverge from each other another 0.01 seconds and then follow similar decay trends. Of key importance is the energy stored in the two rods at the time where the original system partitions into the two separate subsystems described before. The partitioning of the system occurs at the time where the sum of the instantaneous mechanical energy in the second and third rods begins to decrease monotonically (ignoring the abrupt drops due to the neglected energy stored in the second joint). Note that, as discussed before, the second joint actually loosens before the first joint in case l, such that the third rod is separated from the first and second and represents its own subsystem whereas the first

and second rods remain coupled together. Additionally, both joints loosen completely before 0.01 seconds in case k, implying that the system further partitions itself into three separate subsystems. Thus, the following analysis does not apply to cases k or l but does apply to the remaining cases. The exact time of partitioning is different for each case; however, in all cases the first joint loosens completely by 0.004 seconds, such that this time provides a fair basis for comparing the instantaneous mechanical energy in each case. The energies for each case at a time of 0.004 seconds are provided in Table 4.5, which shows that the energies in all cases where the second joint does not loosen are all less than the cases where it does loosen. Thus, we conclude that one factor that determines whether or not a joint loosens after the other one loosens is the amount of energy in the two rods that remain coupled after the partitioning of the system.

Table 4.5 The mechanical energy shared between the second and third rods at 0.004 seconds.

Case	Energy [J]
a	14.39
b	11.37
c	19.26
d	13.92
e	11.36
f	19.98
g	13.13
h	11.58
i	21.44
j	11.98
k	14.67
l	14.06

4.9. Regime V: Complete Rapid Loosening of the First Joint, $P > 380$ kN

The final regime corresponds to forcing cases where the applied force is so strong that the first joint loosens completely regardless of its initial starting torque or that of the second joint. Refer to Figure 4.20 to see the two cases in this regime (a) where it starts showing this behavior and (b) a very large force to showcase how this regime evolves. Thus, in this regime, the behavior of the first joint is independent of the evolution of the second joint; however, the second joint continues to be dependent on the initial torque in the first joint. This dependence is likely due to the amount of energy that remains in the second and third rods after the first joint completely loosens, similar to the behavior in the previous regime. The regime is characterized by strong dependence of the second joint on the first joint for forces below 600 kN and weak dependence above 600 kN. We hypothesize that the weak dependence eventually gives way to total independence around 1200 kN, but this force was not directly investigated given its unrealistic amplitude – it is unlikely that such a force could be realized without permanently deforming the rods in an experiment. Furthermore, we hypothesize that for sufficiently high enough forces, the second joint will not loosen regardless of its initial torque, but such forces are also physically unrealistic and were not investigated in this research.

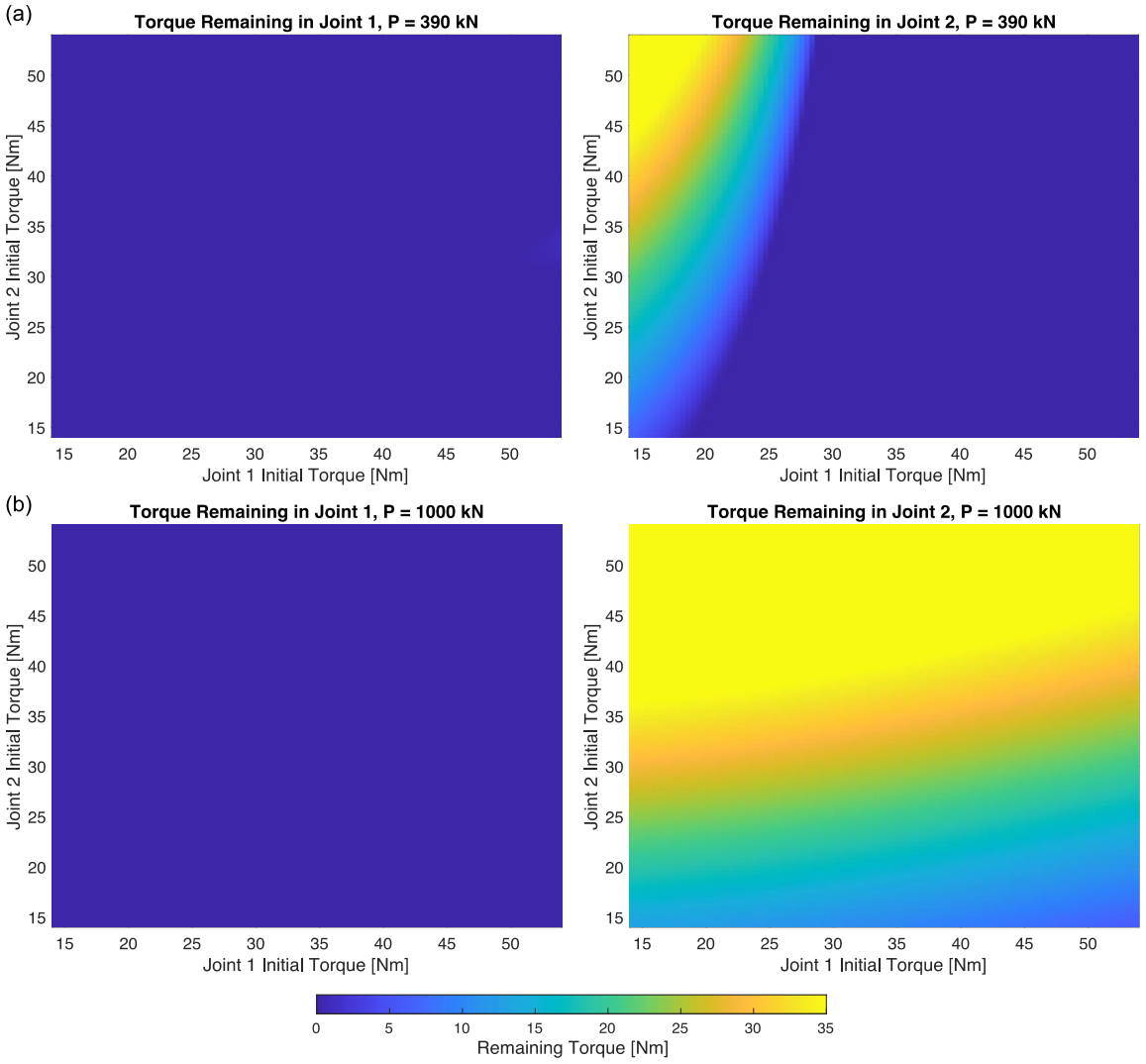

Figure 4.20 The remaining torques in each joint for excitation forces of (a) 390 kN and (b) 1000 kN inside Regime V: Complete Rapid Loosening of the First Joint.

CHAPTER 5-CONCLUSION AND FUTURE WORK

5.1. Concluding Remarks

This thesis investigated the behavior of rods coupled together with axially aligned threaded joints using computational models based on previous split-Hopkinson pressure bar experiments of similar systems. The third chapter introduced the previous experiments and the proposed model for capturing the loosening of axially aligned joints. In each case, the system was excited using a shock excitation with a duration based on previous experiments and variable amplitude. The joints were modeled by treating the instantaneous torques as a new dynamic degrees-of-freedom governed by a first-order differential equation where the rate of loosening depends explicitly on the squared relative velocity across the joint. The coupling stiffness between the rods was modeled as dependent on the torque in the joint using a monotonically increasing function with large slope near zero torque and slope that converges to zero at a theoretical maximum torque. The theoretical maximum torque corresponds to the theoretical maximum possible stiffness which was chosen to be the stiffness of a comparable solid section. The model for the torque-dependent stiffness and the rate of torque loss were identified based on previous experimental measurements and were set equal for every joint considered. The proposed model was applied to a system consisting of two rods and a single joint and the results demonstrated that the proposed model is capable of reproducing experimental measurements in both the instantaneous strains and the amount of total torque lost for each measurement case. It is important to note that the parameters and model used is

found from physical experimentation so for other similar studies to be done on other types of joints or system the parameters will need to be found and verified.

The fourth chapter considered a theoretical system composed of three rods with two joints and investigated the effect of loosening in one joint on the evolution of the other joint. Early simulations of the system revealed that for some combinations of initial torques and forcing amplitude only one of the two joints would loosen completely. To this end, computational simulations for 10000 initial torque combinations were performed for 72 different forcing amplitudes ranging from 5 kN to 1000 kN. These simulations revealed that the behavior of the system can be separated into five different regimes: Regime I: Independence, $0 \leq P \leq 50$ kN; Regime II: Weak Dependence, $50 < P \leq 80$ kN; Regime III: Strong Dependence, $80 < P \leq 120$ kN; Regime IV: Bands of mitigation, $120 < P \leq 380$ kN; and Regime V: Complete Rapid Loosening of the First Joint, $P > 380$ kN. Each of these regimes was investigated in detail and a deeper investigation of the fourth regime revealed that the bands of mitigation resulted from different amounts of energy remaining in the two rods that remain coupled after the one of the joints loosens completely. We hypothesize that the distribution of the energy among the modes governing the remaining coupled rods also plays a role in whether or not the remaining joint loosens completely. However, this line of research is left open for further investigation. The results of this research indicate that for certain sets of initial torques and forces, only one of the joints will completely loosen whereas the other joint maintains some level of preload. This result hints at the possibility of incorporating "dummy" joints into the structure to prevent a vital joint from loosening under a single

shock loading event. We hypothesize that similar behavior could be designed into assembled structures that use lap-type joints instead of axially aligned threaded joints, but this is left open for future work.

5.2. Future Work

As a continuation of this research, physical experiment of comparable three-rod-two-joint systems should be performed in a similar way as the split-Hopkinson pressure bar experiments that were discussed in Chapter 3. These experiments would serve to verify and validate the predictions made in this research and could provide further insight into the underlying mechanisms governing the different regimes observed in Chapter 4. Specifically, it is of key importance to recreate the bands of mitigation as well as the bands of loosening that were observed in the fourth regime as discussed in Chapter 4. Based on the findings of experiments, a similar computational model will need to be created to reproduce the experimental measurements. This will likely lead to additional sets of parameters for the joints instead of only a single set as was used in this research. Moreover, additional experiments should be performed to construct a better identification for the rate of loosening and the torque-dependent stiffness of each joint.

Although it was concluded that the amount of energy remaining in the partitioned systems after one joint loosens is the underlying reason for why the other joint does or does not loosen, further studies are needed to confirm that this is the only underlying mechanism. For example, it is likely that the distribution of the energy across the harmonics (or modes) of the partitioned system also plays a strong role in whether the

joint loosens or does not. As such, the energy distribution across the modes should be investigated using either modal energy obtained by calculating a new stiffness matrix as the joint loosens or using advanced signal decomposition techniques. This would allow one to investigate how energy is distributed across the modes and determine the effect of the distribution on the remaining torque in each joint.

Finally, this research focused entirely on the loosening of axially aligned threaded joints, but it is likely that at least some of the underlying behavior and mechanisms arise for other types of joints, such as bolted lap joints. Future investigations into the loosening of such joints would need to consider the direction of the applied motion as well as the orientation of the bolted joint and how it couples to the rest of the structure. Furthermore, it is likely that the evolution of a single bolt couples to the evolution of all other bolts through changes in the global dynamics of the parent structure. Such interactions should be investigated thoroughly as it is likely that they can be exploited to mitigate loosening This joint is also widely used and has the same issues so understanding this joint would be beneficial. As a continuation of the research on axial joints the next step could be to look at the manipulation of the wave transfer in rods that are in the configuration of a “Y” joint rather than what was discussed in this thesis. The benefit of starting a discussion like the one that this thesis brings up is that the future possibilities could be very impactful in many different scenarios whether it be more computational work or experimental.

References

Alkelani, Ali A., Basil A. Housari, and Sayed A. Nassar. 2008. “A Proposed Model for Creep Relaxation of Soft Gaskets in Bolted Joints at Room Temperature.” *Journal of Pressure Vessel Technology* 130 (1): 011211. https://doi.org/10.1115/1.2826430.

Ampuero, Jean-Paul (2021). SEMLAB (https://www.mathworks.com/matlabcentral/fileexchange/6154-semlab), MATLAB Central File Exchange. Retrieved June 8, 2021.

Bancroft, Dennison. 1941. “The Velocity of Longitudinal Waves in Cylindrical Bars.” *Physical Review* 59 (7): 588–93. https://doi.org/10.1103/PhysRev.59.588.

Basava, S., and D. P. Hess. 1998. “Bolted Joint Clamping Force Variation Due to Axial Vibration.” *Journal of Sound and Vibration* 210 (2): 255–65. https://doi.org/10.1006/jsvi.1997.1330.

Becker, William and Burton E. Becker, Replacement of maxillary and mandibular molars with single endosseous implant restorations: A retrospective study, The Journal of Prosthetic Dentistry. 74 (1995) 51–55. https://doi.org/10.1016/S0022-3913(05)80229-X.

Brake Pedal Bolt Could Come Loose - NHTSA Campaign Number: 21V152000, National Highway Traffic Safety and Administration, Washington, DC, 2021. https://www.nhtsa.gov/recalls?nhtsaId=21V152000.

Bunyan, Jonathan, Keegan J. Moore, Alireza Mojahed, Matthew D. Fronk, Michael Leamy, Sameh Tawfick, and Alexander F. Vakakis. 2018. “Acoustic Nonreciprocity in a Lattice Incorporating Nonlinearity, Asymmetry, and Internal Scale Hierarchy: Experimental Study.” *Physical Review E* 97 (5): 052211. https://doi.org/10.1103/PhysRevE.97.052211.

Chen, Weinong W., and Bo Song. 2011. *Split Hopkinson (Kolsky) Bar : Design, Testing and Applications*. Springer.

CVT Select Lever Cable Nut Not Tightened Properly - NHTSA Campaign Number: 21V024000, National Highway Traffic Safety and Administration, Washington, DC, 2021. https://www.nhtsa.gov/recalls?nhtsaId=21V024000.

“DIN 25201-4: 2010-03 Annex B Test Specification for Demonstrating the Resistance to Self-Loosening of Secured Bolted Joints.” 2010. Berlin: Deutsches Institut für Normung c.V.

“DIN 65151: 2002-08 Dynamic Testing of the Locking Characteristics of Fasteners under Transverse Loading Conditions (Vibration Test).” 2002. Berlin: Deutsches Institut für Normung c.V.

Dinger, G. 2015. “Dynamic Modeling and Simulation of the Screwing Behavior of Thread Forming Screws.” *Journal of Manufacturing Processes* 20 (October): 374–79. https://doi.org/10.1016/j.jmapro.2015.06.012.

Dinger, G., and C. Friedrich. 2011. “Avoiding Self-Loosening Failure of Bolted Joints with Numerical Assessment of Local Contact State.” *Engineering Failure Analysis* 18 (8): 2188–2200. https://doi.org/10.1016/j.engfailanal.2011.07.012.

Dodson, Jacob C., Ryan D. Lowe, Jason R. Foley, Christopher Mougeotte, David Geissler, and Jennifer Cordes. 2014. “Dynamics of Interfaces with Static Initial

Loading." In *Dynamic Behavior of Materials, Volume 1*, edited by Bo Song, Dan Casem, and Jamie Kimberley, 37–50. Conference Proceedings of the Society for Experimental Mechanics Series. Springer International Publishing. https://doi.org/10.1007/978-3-319-00771-7_5.

Dodson, Jacob C., Janet Wolfson, Jason R. Foley, and Daniel J. Inman. 2012. "Transmission of Guided Waves Across Prestressed Interfaces." In *Topics in Nonlinear Dynamics, Volume 3*, edited by D. Adams, G. Kerschen, and A. Carrella, 83–94. Conference Proceedings of the Society for Experimental Mechanics Series. Springer New York. https://doi.org/10.1007/978-1-4614-2416-1_8.

Dominik, Jozef. 2015. "Testing Bolting Resistance to Vibration." *Fastener + Fixing Magazine*, September 2015.

Door Hinge Screws Not Tightened Properly – NHTSA Campaign Number: 21V359000, National Highway Traffic Safety and Administration, Washington, DC, 2021. https://www.nhtsa.gov/recalls?nhtsaId=21V359000.

Ewins, D. J. 2000. *Modal Testing: Theory, Practice, and Application*. Research Studies Press.

Fichtner, Andreas. *Full Seismic Waveform Modelling and Inversion*. 1st ed. 2011., Springer Berlin Heidelberg, 2011, doi:10.1007/978-3-642-15807-0.

Foley, Jason R., Jacob C. Dodson, C. M. McKinnon, V. K. Luk, and G. L. Falbo. 2010. "Split Hopkinson Rod Experiments of Preloaded Interfaces." In *Proceedings of the IMPLAST 2010 Conference*. Society for Experimental Mechanics.

Ford Motor Company Issues Two Safety Recalls in North America, Ford Motor Company, Dearborn, MI, 2018. https://media.ford.com/content/fordmedia/fna/us/en/news/2021/02/18/ford-motor-company-issues-two-safety-recalls.html.

Ford Motor Company Issues Two Safety Recalls in North America, Ford Motor Company, Dearborn, MI, 2021. https://media.ford.com/content/fordmedia/fna/us/en/news/2021/02/18/ford-motor-company-issues-two-safety-recalls.html.

Ford Motor Company to Address Subframe Bolt Issue Affecting Fewer Than 75 Mustang Mach-E Owners, Ford Motor Company, Dearborn, MI, 2021. https://media.ford.com/content/fordmedia/fna/us/en/news/2021/03/05/ford-motor-company-to-address-subframe-bolt-issue.html.

Fort, Valentin, Abdel-Hakim Bouzid, and Michel Gratton. 2018. "Analytical Modeling of Self-Loosening of Bolted Joints." In . American Society of Mechanical Engineers Digital Collection. https://doi.org/10.1115/PVP2018-84016.

Fort, Valentin, Abdel-Hakim Bouzid, and Michel Gratton. . 2019. "Analytical Modeling of Self-Loosening of Bolted Joints Subjected to Transverse Loading." *Journal of Pressure Vessel Technology* 141 (3). https://doi.org/10.1115/1.4042798.

Front Seat Belts Not Securely Attached to B-Pillar – NHTSA Campaign Number: 21V389000, National Highway Traffic Safety and Administration, Washington, DC, 2021.

Fuel Rail Bolts May Loosen Allowing Fuel Leak, National Highway Traffic Safety and Administration, Washington, DC, 2020. https://static.nhtsa.gov/odi/rcl/2020/RCAK-20V648-8465.pdf.

Gong, Hao, Jianhua Liu, and Xiaoyu Ding. 2018. "Study on the Critical Loosening Condition toward a New Design Guideline for Bolted Joints:" *Proceedings of the Institution of Mechanical Engineers, Part C: Journal of Mechanical Engineering Science*, September. https://doi.org/10.1177/0954406218802928.

Gong, Hao. Jianhua Liu, and Xiaoyu Ding. 2021. "Study on Local Slippage Accumulation between Thread Contact Surfaces and Novel Anti-Loosening Thread Designs under Transversal Vibration." *Tribology International* 153 (January): 106558. https://doi.org/10.1016/j.triboint.2020.106558.

Gorham, D. A. 1983. "A Numerical Method for the Correction of Dispersion in Pressure Bar Signals." *Journal of Physics E: Scientific Instruments* 16 (6): 477. https://doi.org/10.1088/0022-3735/16/6/008.

Gray, G. T. 2000. "Classical Split Hopkinson Pressure Rod Technique." In *Mechanical Testing and Evaluation*, edited by H. Kuhn and D. Medlin. Vol. 8. ASM Handbook. Materials Park, OH: ASM International.

Hess, D. P. 1996. "Threaded Components Under Axial Harmonic Vibration, Part 2: Kinematic Analysis." *Journal of Vibration and Acoustics* 118 (3): 423–29. https://doi.org/10.1115/1.2888200.

Hess, D. P., and K. Davis. 1996. "Threaded Components Under Axial Harmonic Vibration, Part 1: Experiments." *Journal of Vibration and Acoustics* 118 (3): 417–22. https://doi.org/10.1115/1.2888199.

Hess, D. P., and S. V. Sudhirkashyap. 1996. "Dynamic Analysis of Threaded Fasteners Subjected to Axial Vibration." *Journal of Sound and Vibration* 193 (5): 1079–90. https://doi.org/10.1006/jsvi.1996.0333.

Hess, D. P., and . 1997. "Dynamic Loosening and Tightening of a Single-Bolt Assembly." *Journal of Vibration and Acoustics* 119 (3): 311–16. https://doi.org/10.1115/1.2889725.

Holmes, H. 1988 Seeking the Perfect Locking Method for Threaded Fasteners, Automation. 35 28–30.

Hood Hinge Scews May Come Loose - NHTSA Campaign Number: 21V107000, National Highway Traffic Safety and Administration, Washington, DC, 2021. https://www.nhtsa.gov/recalls?nhtsaId=21V107000.

Hopkinson, B. 1914. "A Method of Measuring the Pressure Produced in the Detonation of High Explosives or by the Impact of Bullets." *Philosophical Transactions of the Royal Society of London Series A-Containing Papers of a Mathematical or Physical Character* 213 (February): 437–56. https://doi.org/10.1098/rsta.1914.0010.

Housari, Basil A., and Sayed A. Nassar. 2007. "Effect of Thread and Bearing Friction Coefficients on the Vibration-Induced Loosening of Threaded Fasteners." *Journal of Vibration and Acoustics* 129 (4): 484–94. https://doi.org/10.1115/1.2748473.

Ibrahim, R. A., and C. L. Pettit. 2005. "Uncertainties and Dynamic Problems of Bolted Joints and Other Fasteners." *Journal of Sound and Vibration* 279 (3): 857–936. https://doi.org/10.1016/j.jsv.2003.11.064.

Incorrect Wheel Nuts May Cause Wheel Separation – NHTSA Campaign Number: 21V86000, National Highway Traffic Safety and Administration, Washington, DC, 2021. https://www.nhtsa.gov/recalls?nhtsaId=21V186000&refurl=rss.

"ISO 16130:2015 Dynamic Testing of the Locking Behaviour of Bolted Connections under Transverse Loading Conditions (Vibration Test)." 2015. Geneva: International Organisation for Standardization.

Izumi, Satoshi, Masatake Kimura, and Shinsuke Sakai. 2007. "Small Loosening of Bolt-Nut Fastener Due to Micro Bearing-Surface Slip: A Finite Element Method Study." *Journal of Solid Mechanics and Materials Engineering* 1 (11): 1374–84. https://doi.org/10.1299/jmmp.1.1374.

Izumi, Satoshi, Takashi Yokoyama, Atsushi Iwasaki, and Shinsuke Sakai. 2005. "Three-Dimensional Finite Element Analysis of Tightening and Loosening Mechanism of Threaded Fastener." *Engineering Failure Analysis* 12 (4): 604–15. https://doi.org/10.1016/j.engfailanal.2004.09.009.

Jiang, Yanyao, Ming Zhang, and Chu-Hwa Lee. 2003. "A Study of Early Stage Self-Loosening of Bolted Joints." *Journal of Mechanical Design* 125 (3): 518–26. https://doi.org/10.1115/1.1586936.

Junker, Gerhard H. 1969. "New Criteria for Self-Loosening of Fasteners Under Vibration." *SAE Transactions* 78: 314–35.

Junker, Gerhard H. 1972. "Criteria for Self Loosening of Fasteners under Vibration." *Aircraft Engineering and Aerospace Technology* 44 (10): 14–16. https://doi.org/10.1108/eb034949.

Kaminskaya V., A. Lipov. 1990. Self-loosening of bolted joints in machine tools during service, Metal Cutting Machine Tools. 12 81–85.

Kasei, Shinji. 2007. "A Study of Self-Loosening of Bolted Joints Due to Repetition of Small Amount of Slippage at Bearing Surface." *Journal of Advanced Mechanical Design, Systems, and Manufacturing* 1 (3): 358–67. https://doi.org/10.1299/jamdsm.1.358.

Kim Saang Bum, Spencer B. F., and Yun Chung-Bang. 2005. "Frequency Domain Identification of Multi-Input, Multi-Output Systems Considering Physical Relationships between Measured Variables." *Journal of Engineering Mechanics* 131 (5): 461–72. https://doi.org/10.1061/(ASCE)0733-9399(2005)131:5(461).

Kolsky, H. 1949. "An Investigation of the Mechanical Properties of Materials at Very High Rates of Loading." *Proceedings of the Physical Society. Section B* 62 (11): 676–700. https://doi.org/10.1088/0370-1301/62/11/302.

Kurt, Mehmet, Melih Eriten, D. Michael McFarland, Lawrence A. Bergman, and Alexander F. Vakakis. 2015. "Methodology for Model Updating of Mechanical Components with Local Nonlinearities." *Journal of Sound and Vibration* 357 (November): 331–48. https://doi.org/10.1016/j.jsv.2015.07.012.

Liu, Jianhua, Huajiang Ouyang, Zhiqiang Feng, Zhenbing Cai, Xuetong Liu, and Minhao Zhu. 2017a. "Study on Self-Loosening of Bolted Joints Excited by Dynamic Axial Load." *Tribology International* 115 (November): 432–51. https://doi.org/10.1016/j.triboint.2017.05.037.

Liu, Jianhua, Huajiang Ouyang, Zhiqiang Feng, Zhenbing Cai, Jinfang Peng, Yongqiang Du, and Minhao Zhu. 2019. "Self-Loosening of Bolted L-Stub Connections under

a Cyclic Separating Load." *Wear*, 22nd International Conference on Wear of Materials, 426–427 (April): 662–75. https://doi.org/10.1016/j.wear.2018.12.023.

Liu, Xuetong, Xue Mi, Jianhua Liu, Laohu Long, Zhenbing Cai, Jiliang Mo, Jinfang Peng, and Minhao Zhu. 2021. "Axial Load Distribution and Self-Loosening Behavior of Bolted Joints Subjected to Torsional Excitation." *Engineering Failure Analysis* 119 (January): 104985. https://doi.org/10.1016/j.engfailanal.2020.104985.

Lozier, M. EQ-4b Global Hawk, T/N 04-2017, 2012.

Loose Brake Caliper Bolts – NHTSA Campaign Number: 21V387000, National Highway Traffic Safety and Administration, Washington, DC, 2021. https://www.nhtsa.gov/recalls?nhtsaId=21V387000.

Loose Steering Column Shaft - NHTSA Campaign Number: 21V031000, National Highway Traffic Safety and Administration, Washington, DC, 2021. https://www.nhtsa.gov/recalls?nhtsaId=21V031000.

Materson, Patrick 194,000 2018-2020 Buick, Cadillac, Chevrolet and GMC Vehicles Recalled for Transmission Issue, Cars.Com. (2020). https://www.cars.com/articles/194000-2018-2020-buick-cadillac-chevrolet-and-gmc-vehicles-recalled-for-transmission-issue-429657/.

Mo, Yimin, Shenghui Guo, Xiongzhen Qin, Jialiang Qin, Kui Zhan, and Xinshang Gao. 2020. "Research on the Numerical Calculation Method for Antiloosening Performance of Screwed Joints under Complex Working Conditions." Research Article. Mathematical Problems in Engineering. Hindawi. May 12, 2020. https://doi.org/10.1155/2020/5915173.

Moore, K. J., J. Bunyan, S. Tawfick, O.V. Gendelman, L. Shuangbao, M. J. Leamy, and A. F. Vakakis. 2018. "Non-Reciprocity in the Dynamics of Coupled Oscillators with Nonlinearity, Asymmetry and Scale Hierarchy." *Phys. Rev. E* 97 (1): 012219.

Moore, K. J., M. Kurt, M. Eriten, J. C. Dodson, J. R. Foley, J. C. Wolfson, D. M. McFarland, L. A. Bergman, and A. F. Vakakis. 2017. "Nonlinear Parameter Identification of a Mechanical Interface Based on Primary Wave Scattering." *Experimental Mechanics* 57 (9): 1495–1508. https://doi.org/10.1007/s11340-017-0320-0.

Motor Mount Fasteners May Loosen Over Time - NHTSA Campaign Number: 20V788000, National Highway Traffic Safety and Administration, Washington, DC, 2020. https://www.nhtsa.gov/recalls?nhtsaId=20V788.

Nah, Hwan-Seon, Hyeon-Ju Lee, and Sung-Mo Choi. 2014. "Evaluating Long-Term Relaxation of High Strength Bolts Considering Coating on Slip Faying Surface." *Steel and Composite Structures* 16 (6): 703–18. https://doi.org/10.12989/scs.2014.16.6.703.

Nah, Hwan-Seon, Hyeon-Ju Lee, Jae-Yong Ryoo, and Sung-Mo Choi. 2012. "Estimation of Long Term Clamping Force of High Strength Bolts By Coating Thickness Parameters of Slip Faying Surfaces." *Journal of the Korean Society for Advanced Composite Structures* 3 (1): 8–15. https://doi.org/10.11004/kosacs.2012.3.1.008.

Nassar, Sayed A., and Antoine Abboud. 2009. “An Improved Stiffness Model for Bolted Joints.” *Journal of Mechanical Design* 131 (12). https://doi.org/10.1115/1.4000212.

Nassar, Sayed A., and Ali A. Alkelani. 2005. “Clamp Load Loss Due to Elastic Interaction and Gasket Creep Relaxation in Bolted Joints.” *Journal of Pressure Vessel Technology* 128 (3): 394–401. https://doi.org/10.1115/1.2218343.

Nassar, Sayed A., and Basil A. Housari. 2005. “Effect of Thread Pitch and Initial Tension on the Self-Loosening of Threaded Fasteners.” *Journal of Pressure Vessel Technology* 128 (4): 590–98. https://doi.org/10.1115/1.2349572.

Nassar, Sayed A., and Basil A. Housari. 2006. “Study of the Effect of Hole Clearance and Thread Fit on the Self-Loosening of Threaded Fasteners.” *Journal of Mechanical Design* 129 (6): 586–94. https://doi.org/10.1115/1.2717227.

Nassar, Sayed A., and Xianjie Yang. 2007. “Novel Formulation of the Tightening and Breakaway Torque Components in Threaded Fasteners.” *Journal of Pressure Vessel Technology* 129 (4): 653–63. https://doi.org/10.1115/1.2767354.

Nassar, Sayed A., and Xianjie Yang. 2008. “Torque-Angle Formulation of Threaded Fastener Tightening.” *Journal of Mechanical Design* 130 (2). https://doi.org/10.1115/1.2821388.

Nassar, Sayed A., and Xianjie Yang. 2009. “A Mathematical Model for Vibration-Induced Loosening of Preloaded Threaded Fasteners.” *Journal of Vibration and Acoustics* 131 (2): 021009-021009–13. https://doi.org/10.1115/1.2981165.

National Instruments. 2003. “NI PXI-6133 Specifications.” National Instruments, Austin.

Nechache, Akli, and Abdel-Hakim Bouzid. 2007. “Creep Analysis of Bolted Flange Joints.” *International Journal of Pressure Vessels and Piping* 84 (3): 185–94. https://doi.org/10.1016/j.ijpvp.2006.06.004.

Noda, Nao-Aki, Xin Chen, Yoshikazu Sano, Magd Abdel Wahab, Hikaru Maruyama, Ryota Fujisawa, and Yasushi Takase. 2016. “Effect of Pitch Difference between the Bolt–Nut Connections upon the Anti-Loosening Performance and Fatigue Life.” *Materials & Design* 96 (April): 476–89. https://doi.org/10.1016/j.matdes.2016.01.128.

Noda, Nao-Aki, Xi Liu, Yoshikazu Sano, Kosuke Tateishi, Biao Wang, Yuto Inui, and Yasushi Takase. 2020. “Prevailing Torque and Residual Prevailing Torque of Bolt-Nut Connections Having Slight Pitch Difference.” *Mechanics Based Design of Structures and Machines* 0 (0): 1–14. https://doi.org/10.1080/15397734.2020.1768114.

Olsen, Heather and Eric Kennedy 2018. Final Report for CPSC on the National Study of Public Playground Equipment and Surfacing, University of Northern Iowa

Olsen, Heather and Eric Kennedy, Safety of School Playgrounds: Field Analysis From a Randomized Sample, The Journal of School Nursing. 36 (2020) 369–375. https://doi.org/10.1177/1059840519827364.

Pai, N. G., and D. P. Hess. 2002a. “Experimental Study of Loosening of Threaded Fasteners Due to Dynamic Shear Loads.” *Journal of Sound and Vibration* 253 (3): 585–602. https://doi.org/10.1006/jsvi.2001.4006.

Part 573 Safety Recall Report 20V-648, National Highway Traffic Safety and Administration, Washington, DC, 2020. https://static.nhtsa.gov/odi/rcl/2020/RCLRPT-20V648-4094.PDF.

Part 573 Safety Recall Report 20V-668, National Highway Traffic Safety and Administration, Washington, DC, 2020. https://static.nhtsa.gov/odi/rcl/2020/RCLRPT-20V668-5029.PDF.

Part 573 Safety Recall Report 20V-709, National Highway Traffic Safety and Administration, Washington, DC, 2020. https://static.nhtsa.gov/odi/rcl/2020/RCLRPT-20V709-9285.PDF.

Pai, Niranjan G., Daniel P. Hess. 2002b. "Three-Dimensional Finite Element Analysis of Threaded Fastener Loosening Due to Dynamic Shear Load." *Engineering Failure Analysis* 9 (4): 383–402. https://doi.org/10.1016/S1350-6307(01)00024-3.

Pichoff, Franck, Matthieu Kummel, and Morten Schiff. 2018. "Dynamic Vibration Testing of Fasteners: Fastener Self-Loosening Theory, Vibration Testing Practical Applications, Comparison of the International Standards and Recommendations on How to Set-up a Meaningful Testing Protocol." *Matériaux & Techniques* 106 (3): 307. https://doi.org/10.1051/mattech/2018029.

Precision Filters, Inc. 2009. "Precision 28144 Quad-Channel Wideband Transducer Conditioner with Voltage and Current Excitation (Datasheet)." Precision Filters, Inc., Ithaca.

Rashquinha, I.A., and D.P. Hess. 1997. "Modelling Nonlinear Dynamics of Bolted Assemblies." *Applied Mathematical Modelling* 21 (12): 801–9. https://doi.org/10.1016/S0307-904X(97)00107-8.

Rear Axle U-Bolt Not Properly Tightened – NHTSA Campaign Number: 21V1940000, National Highway Traffic Safety and Administration, Washington, DC, 2021. https://www.nhtsa.gov/recalls?nhtsaId=21V194000.

Rear Stabilizer Bracket Bolts May Detach – NHTSA Campaign Number: 21V263000, National Highway Traffic Safety and Administration, Washington, DC, 2021. https://www.nhtsa.gov/recalls?nhtsaId=21V263000.

Riveros, Guillermo A., Hussam Mahmoud, and Santiago Rodriguez Lopez. 2016. "Causes of Pretension Loss in High-Strength Bolts." https://erdc-library.erdc.dren.mil/xmlui/handle/11681/20263.

Safety Recall 4420F: 2020 CX-30 and 2020 Mazda3 Front Brake Caliper Bolts May Loosen, National Highway Traffic Safety and Administration, Washington, DC, 2020. https://static.nhtsa.gov/odi/rcl/2020/RCRIT-20V346-5901.pdf.

Schiff, Morten. 2019. "Beyond Junker: A Paradigm Shift in Validating and Optimising Bolted Joints." *Fastener + Fixing Magazine*, March 4, 2019. https://www.fastenerandfixing.com/manufacturing-technology/beyond-junker-a-paradigm-shift-in-validating-and-optimising-bolted-joints/.

Sears, Gary, and David King. 2004. "Joint Integrity Management of Critical Flanges." *International Journal of Pressure Vessels and Piping*, The 7th International Conference on Operating Pressure Equipment, 81 (6): 513–19. https://doi.org/10.1016/j.ijpvp.2003.12.021.

Seat Belt Retractor Not Securely Attached – NHTSA Campaign Number: 21V388000, National Highway Traffic Safety and Administration, Washington, DC, 2021. https://www.nhtsa.gov/recalls?nhtsaId=21V388000.

Shoji, Yasumasa, and Toshiyuki Sawa. 2005. "Analytical Research on Mechanism of Bolt Loosening Due to Lateral Loads." In , 59–65. American Society of Mechanical Engineers. https://doi.org/10.1115/PVP2005-71333.

Silva, Júlio M. M. 1999. *Modal Analysis and Testing*. Dordrecht: Springer Netherlands.

Song, Y., C.J. Hartwigsen, D.M. McFarland, A.F. Vakakis, and L.A. Bergman. 2004. "Simulation of Dynamics of Beam Structures with Bolted Joints Using Adjusted Iwan Beam Elements." *Journal of Sound and Vibration* 273 (1–2): 249–76.

Suspension Components Not Tightened Properly – NHTSA Campaign Number: 21V157000, National Highway Traffic Safety and Administration, Washington, DC, 2021. https://www.nhtsa.gov/recalls?nhtsaId=21V157000&refurl=rss.

Technical investigation report on the derailment of the intercity train #3567 on July 12, 2013 in Brétigny-sur-Orge, French Land Transport Accident Investigation Bureau, 2015.

Tendo, Masayuki, Kenji Yamada, and Yasumi Shimura. 2000. "Stress Relaxation Behavior at High-Tension Bolted Connections of Stainless-Steel Plates." *Journal of Engineering Materials and Technology* 123 (2): 198–202. https://doi.org/10.1115/1.1338481.

Top 10 Health Technology Hazards for 2020: Expert Insights from Health Devices, Emergency Care Research Institute, 2020.

Wu, X., J. Shi, J. Wu, Y. Cheng, K. Peng, J. Chen, H. Jiang, Pedicle screw loosening: the value of radiological imagings and the identification of risk factors assessed by extraction torque during screw removal surgery, Journal of Orthopaedic Surgery and Research. 14 (2019) 6. https://doi.org/10.1186/s13018-018-1046-0.

Yang Jun and DeWolf John T. 1999. "Mathematical Model for Relaxation in High-Strength Bolted Connections." *Journal of Structural Engineering* 125 (8): 803–9. https://doi.org/10.1061/(ASCE)0733-9445(1999)125:8(803).

Yang, Xianjie, and Sayed Nassar. 2011a. "Vibration-Induced Loosening Performance of Preloaded Threaded Fasteners." In , 129–38. American Society of Mechanical Engineers Digital Collection. https://doi.org/10.1115/PVP2010-25811.

Yang, Xianjie, and Sayed A. Nassar. {Citation}2011b. "Analytical and Experimental Investigation of Self-Loosening of Preloaded Cap Screw Fasteners." *Journal of Vibration and Acoustics* 133 (3). https://doi.org/10.1115/1.4003197.

Yang, Xianjie, and Sayed A. Nassar. 2013. "Deformation and Slippage Modeling for Investigating Bolt Loosening Under Harmonic Transverse Excitation." In , 321–32. American Society of Mechanical Engineers Digital Collection. https://doi.org/10.1115/PVP2012-78367.

Yang, Xianjie, Sayed A. Nassar, and Zhijun Wu. 2011. "Criterion for Preventing Self-Loosening of Preloaded Cap Screws Under Transverse Cyclic Excitation." *Journal of Vibration and Acoustics* 133 (4). https://doi.org/10.1115/1.4003596.

Yang, Xianjie, Sayed A. Nassar, Zhijun Wu, and Aidong Meng. 2012. "Nonlinear Behavior of Preloaded Bolted Joints Under a Cyclic Separating Load." *Journal of Pressure Vessel Technology* 134 (1). https://doi.org/10.1115/1.4004614.

Yokoyama, Takashi, Mårten Olsson, Satoshi Izumi, and Shinsuke Sakai. 2012. "Investigation into the Self-Loosening Behavior of Bolted Joint Subjected to Rotational Loading." *Engineering Failure Analysis* 23 (July): 35–43. https://doi.org/10.1016/j.engfailanal.2012.01.010.

Zadoks, R. I., and X. Yu. 1997. "AN INVESTIGATION OF THE SELF-LOOSENING BEHAVIOR OF BOLTS UNDER TRANSVERSE VIBRATION." *Journal of Sound and Vibration* 208 (2): 189–209. https://doi.org/10.1006/jsvi.1997.1173.

Zhang, Ming, Yanyao Jiang, and Chu-Hwa Lee. 2006. "Finite Element Modeling of Self-Loosening of Bolted Joints." *Journal of Mechanical Design* 129 (2): 218–26. https://doi.org/10.1115/1.2406092.

Zhang, Mingyuan, Liantao Lu, Wenjian Wang, and Dongfang Zeng. 2018. "The Roles of Thread Wear on Self-Loosening Behavior of Bolted Joints under Transverse Cyclic Loading." *Wear* 394–395 (January): 30–39. https://doi.org/10.1016/j.wear.2017.10.006.

Zhang, Mingyuan, Dongfang Zeng, Liantao Lu, Yuanbin Zhang, Jing Wang, and Jingmang Xu. 2019. "Finite Element Modelling and Experimental Validation of Bolt Loosening Due to Thread Wear under Transverse Cyclic Loading." *Engineering Failure Analysis* 104 (October): 341–53. https://doi.org/10.1016/j.engfailanal.2019.05.001.

Zhu, Linbo, Jun Hong, and Xiangjun Jiang. 2016. "On Controlling Preload and Estimating Anti-Loosening Performance in Threaded Fasteners Based on Accurate Contact Modeling." *Tribology International* 95 (March): 181–91. https://doi.org/10.1016/j.triboint.2015.11.006.